Dalton Transactions

ROYAL SOCIETY OF CHEMISTRY

PAPER

View Article Online
View Journal

Cite this: DOI: 10.1039/d6dt01002d

The design of earth abundant metal catalysts for nitrous oxide-based oxidations: Part I. N_2O coordination and oxygen-transfer to metal

Kenneth M. Nicholas

Nitrous oxide (N_2O) is thermodynamically unstable, but kinetically unreactive, and thus presents a fundamental challenge for catalysis. It is also a potent greenhouse gas, yet it is underutilized as a chemical feedstock and thus provides a practical opportunity for catalysis as well. A computational design approach is employed in this first part of a two-part study to evaluate the potential of selected first row transition metal complexes to activate N_2O as an oxidant for various substrates. Density Functional Theory (DFT) calculations are employed on several ligated transition metal fragments LM, M = V(III), Fe(II), Mn(II), Cr(II), Cu(I) and second row Ru(II) with 4/5-coordinate geometries to assess their N_2O binding affinity and energetics for N–O cleavage to LMO. The effects of the ligand, coordination number, the metal, its spin state, charge, *etc*. are addressed. The key points from the DFT analysis and energy profiles are: (1) favorable N_2O binding (ΔG_a < 0) is correctly predicted for known N_2O complexants: (*N*-3Pyr)V, $[Al(OR_F)_4]Cu$ and $(NH_3)_5Ru^{2+}$; (2) for a range of unproven complexants, the N_2O-affinity ranges from moderate (ΔG_a −5 to +2 kcal mol^{-1}) to low (ΔG_a > +5 kcal) in the order Cr(II) > Ru(II) ≥ Fe(II) ≅ Mn(II) ≅ Cu(I); (3) M–N binding to N_2O is generally more stable than M–O binding, but is nearly isoenergetic for many high spin metal fragments; (4) N–O cleavage *via* monometallic complexes, LM–ON_2 (M = Fe(II), Mn(II), Cu(I)) requires moderate-to-high activation energies, $\Delta G^*_{N\text{--}O}$ (23–40 kcal mol^{-1}), but the barriers are much lower for LCr(II) and LRu(II) species (3–17 kcal mol^{-1}); (5) N–O cleavage is facilitated by pyramidal and penta-coordinating ligands; (6) $\Delta G^*_{N\text{--}O}$ from *bent* N_2O-bimetallics is very low: 1–5 kcal mol^{-1}; and (7) the total activation energy barriers ΔG^*_{span} for bimetallic-N_2O complexes, *ca.* 20–30 kcal mol^{-1}, are 5–8 kcal mol^{-1} lower than for mono-metallics, providing a bimetallic advantage for N_2O scission to oxido-metals, LM=O.

Received 29th April 2026,
Accepted 28th May 2026

DOI: 10.1039/d6dt01002d

rsc.li/dalton

Introduction

Nitrous oxide (N_2O) is an abundant, atmospheric component with rather limited commercial use, including as a mild anesthetic ('laughing gas'), a fuel enhancer ('nitro') and an aerosol propellant. These uses of nitrous oxide are dwarfed by its emissions from both natural and man-made sources. It is emitted predominantly by biological sources[1] in soil and water and secondarily from diesel vehicle exhaust[2] and in nylon production.[3] Nitrous oxide is an important long-lived greenhouse gas, approximately 300 times more potent than carbon dioxide, contributing significantly to global warming.[4] The atmospheric levels of N_2O have been rising, primarily due to the surging use of fertilizers to meet the food needs of a growing global population. The impacts of this imbalance between N_2O emission and utilization calls for solutions that increase its chemical utilization and/or destruction.

Nitrous oxide is thermodynamically unstable with respect to its decomposition products, N_2 and O_2 (ΔG_{dec} −26 kcal mol^{-1}).[5] However, N_2O decomposition and many of its other potential chemical transformations are kinetically challenging for a lack of established low barrier energy pathways. The most important known *catalyzed* reactions of N_2O are its decomposition and NH_3 reduction relevant to diesel exhaust and environmental mitigation,[6] typically conducted over solid iron- and copper-zeolite catalysts operating at temperatures >300 °C.[7] The Solomon and Sels team have performed valuable experimental and computational analysis of the binding, activation and conversion of N_2O on these supported catalysts. The Cu-zeolites were suggested to contain structurally diverse active sites for both mono and bi-metallic binding; in particular, Cu_2O sites with O,O- or N,O-bridged bimetallic binding modes provide the lowest energy N–O scission pathways (ΔH^* *ca.* 5 kcal mol^{-1}).[8] For Fe-zeolite beta, a monometallic Fe(II) site has been implicated to bind N_2O in a terminal fashion (N-

Department of Chemistry and Biochemistry, University of Oklahoma, Norman, OK 73019, USA. E-mail: knicholas@ou.edu

or O-), the latter of which transforms to Fe(IV)=O site with a higher activation enthalpy of 25 kcal mol^{-1}.[9] For the decomposition reaction, O_2 evolution from the oxidized M–O site is likely turnover-limiting. However, the structural heterogeneity and immutability of the active sites in these solid catalysts impede rational performance improvement. In a recent study, we reported computational modeling of several potential molecular (homogeneous) catalysts for nitrous oxide decomposition and proposed the viability of low temperature catalytic N_2O-splitting by Ru(Cl)(POR).[10]

Reduction of nitrous oxide (to N_2 and H_2O) occurs naturally under ambient conditions in some plants, as catalyzed by the enzyme nitrous oxide reductase (*N_2OR*).[11] This biocatalyst has a novel protein-bound Cu_4S active site,[12] at which N_2O was suggested to engage in multicenter binding and activation,[13] but the detailed pathway to dinitrogen and water remains unknown. Structural and, more recently, functional model compounds for the Cu_4S active have been developed, by the Mankad[14] and Tolman[15] groups. In the realm of synthetic molecular catalysts for N_2O reduction, the Millstein group has reported a Ru(II)–pincer complex that catalyzes the hydrogenation and hydrosilation of N_2O.[16] The electrocatalytic reduction of N_2O by synthetic catalysts has received increasing attention, employing both solid and homogeneous transition metal-based catalysts.[17] Generally, in these systems a reduced form of the metal species, *e.g.* Fe(I,0) and Co(I), has been implicated in the transient coordination and transformation of N_2O. In some instances, it appears that bimetallic centers can moderate kinetic barriers, as in an earlier study by Collman *et al.* showing the accelerated electrocatalytic reduction of N_2O by tethered bimetallic cobalt-porphyrins.[18] Detailed mechanistic pathways and structure/activity relationships for these electrocatalytic systems are yet to be established.

Outside of catalytic decomposition and reduction reactions, other catalytic transformations of N_2O are rather undeveloped. A few early reports of homogeneous metal-catalyzed oxidations with N_2O have been published involving Ru(porphyrin) species, including (TTP)RuO_2-promoted benzylic hydrocarbon hydroxylation,[19] benzylic alcohol oxidation[20] and alkene epoxidation,[21] presumably *via* (POR)$Ru(O_{0,1})(N_2O)$ intermediates (Fig. 1). Newer additions to the realm of transition metal-based catalytic transformations of N_2O are C–X (aryl halide) to C–O (aryloxide) substitutions enabled by low valent Ni-complexes.[22]

The design and development of catalysts for various nitrous oxide conversions could benefit significantly from an enhanced fundamental knowledge and understanding of the interaction and reactions of N_2O with metallic and other potentially activating species. Several reports have shown that nitrous oxide can react directly with powerful nucleophiles[23] such as amide[24] and hydrazide salts,[25] organo-metals,[26] N-heterocyclic carbenes[27] and phosphines[28] to form N-bound adducts (Fig. 2A) or can transfer its oxygen atom to the nucleophile (Fig. 2A). Reactions of N_2O with frustrated Lewis pairs (FLP), which typically incorporate a nucleophilic and an electrophilic center, produce adducts, which can feature a distinctly bent N_2O bridge and an elongated (presumably weaker) N–O bond (Fig. 2B).[29]

All the structurally confirmed N_2O–metal complexes exhibit one of two binding modes: terminal N-binding (η^1-N) or side-on N–N binding (η^2-N,N) (Fig. 3).[30] In the η^1-N mode, the M–N_2O unit is essentially linear and the bond lengths of the coordinated N_2O unit are rather little changed from free N_2O (*vide infra*), suggesting little electronic perturbation of the N_2O fragment.[31a–c] In the η^2-N,N mode the N_2O unit is substantially bent (*ca.* 130°) and the N–N bond is elongated, indicative of substantial modification of the electronic character of the N_2O unit.[32] Although the number of examples is still small, the metal centers in these molecules are in low-to-middle oxidation states, *i.e.* have metal fragments that are relatively electron rich. It is noteworthy that although M(η^1-O-N_2) coordination has been proposed or assumed in O-transfer reactions of N_2O with low oxidation state metal-complexes, no direct experimental evidence has been reported for such species.

In addition to the formation of metal–N_2O complexes, a highly reduced metal species, *e.g.* ligated Ti(III),[33] V(III),[34] U(III),[35] Ru(II),[36] can abstract the O-atom from N_2O to produce an oxido-metal, LMO, and dinitrogen (Fig. 4). The presumed metal–N_2O intermediates in these oxidations have not been identified. Such O-transfer oxidations of electron rich metal-species are analogous to those of non-metallic nucleophiles (Fig. 2a). Another class of reactions between N_2O and tran-

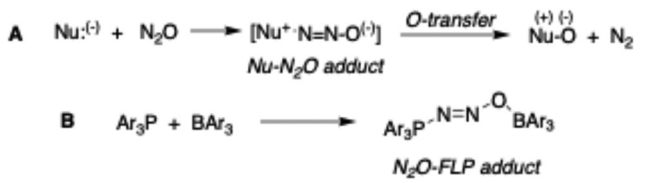

Fig. 2 Reactions between N_2O and nucleophiles (A) and FLPs (B).

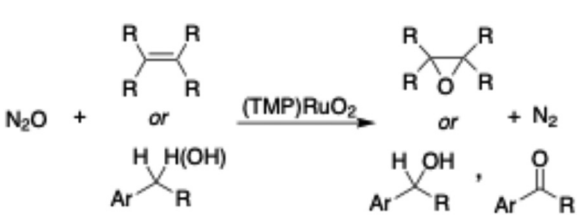

Fig. 1 Catalytic oxidations by N_2O with (POR)RuO_2.

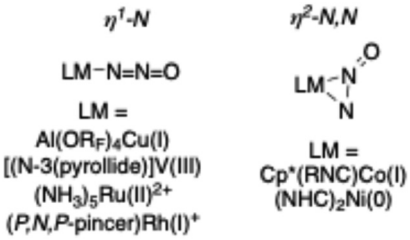

Fig. 3 Structurally established modes of nitrous oxide coordination.

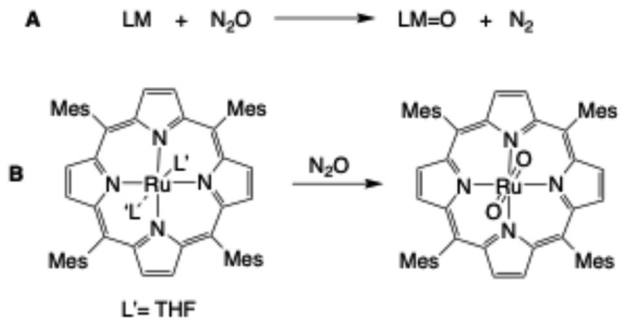

Fig. 4 O-transfer oxidation of metal-based species by N_2O. (A) General equation; (B) N_2O-deoxygenation by (TMP)Ru(THF)$_2$.[36]

sition metal complexes is insertion into metal–carbon bonds, which results in O-transfer to carbon or the metal as illustrated by Hillhouse and coworkers.[37]

There is a scarcity of systematic, broad scope experimental and theoretical studies of the interaction and transformations of N_2O with potential transition metal activators.[23,30] We are especially interested in evaluating the factors that affect the viability of schemes that utilize N_2O as a reagent for oxygen atom-transfer (OAT, oxidation) and nitrogenation reactions. The reports of Ru-promoted hydrocarbon oxidation by N_2O stimulated our conception of a general two-stage catalytic pathway for substrate (*e.g.* hydrocarbon) oxidation by earth-abundant transition metals, wherein initially N_2O transfers its O-atom to a LM-fragment to form a reactive LMO (oxido) species (releasing N_2), which, in turn, can oxidize the substrate (Fig. 5). For practical, economic reasons we are particularly interested in developing such processes with earth-abundant metal-centered catalysts. In the present study, we employ DFT calculations on several divalent metal fragments LM, M^{II} = Fe, Mn, Cr, Ru and Cu^{I} having common 4/5-coordinating ligands to assess their N_2O binding affinity, the structures and energies of the resulting metal complexes, LM(N_2O), and the energetics of N–O cleavage to LMO to reveal the effects of the ligand, coordination number, the metal, its spin state, charge,

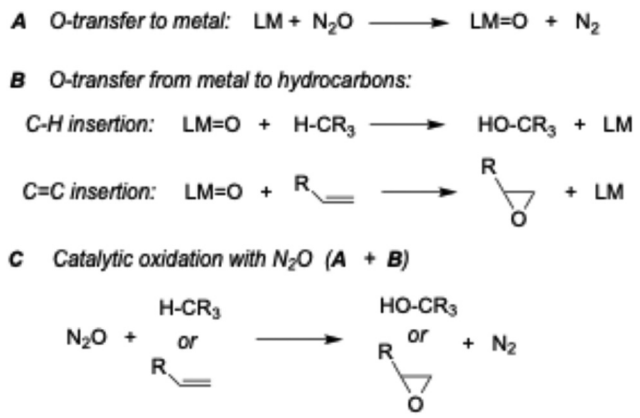

Fig. 5 Rebound pathway *via* oxido-metals (A + B) for catalytic oxidations with N_2O (C).

etc. (Fig. 5A). In a subsequent report, we will evaluate the potential for hydrocarbon oxidation by the derived LMO species (Fig. 5B) and gauge the overall kinetic viability of rebound oxidation energetics according to the scheme in Fig. 5. Instead of the typical, empirical, hit-or-miss and often inefficient approach to reaction discovery and catalyst development, we present here a *predictive* computational study of catalyst design and virtual screening, seeking the development of new catalytic reactions of nitrous oxide.

Computational methods

DFT methods, when applied to transition metal complexes, are widely recognized for their structural accuracy, reasonable prediction of many electronic properties and ligand dissociation energies, at a relatively low computational cost.[38] Presently, however, there are no universally proven methods that will provide accurate spin-dependent energies for odd-electron (open-shell) transition metal species.[39] For Fe(II,III) and, to a lesser extent, other open-shell first row transition metals, several studies have shown that the B3LYP (hybrid functional)[40] and OPBE[41] functionals are usually reliable for determining ground state spin multiplicities, but methods for obtaining accurate energies of higher states are still being sought.[42] Since many transition metal complexants (fragments) are coordinatively unsaturated, they are inherently reactive/unstable and their ground spin states are often experimentally unknown.

With the above issues in mind, quantum electronic calculations were carried out using the Gaussian 16 software suite.[43] Unless otherwise specified, all structure optimizations were performed using the B3LYP functional,[44] with the LANL2DZ basis set on the metal[45] and 6-31G(d) for 1st and 2nd row atoms and 6-311+G(d,p) for 3rd row non-metal atoms.[46] Following B3LYP geometry optimization and frequency calculation, corrections for dispersion and solvation were applied in single point energy calculation using the D3 dispersion[47] and SMD solvation[48] methods to give the free energy (G) values in solution. For almost all species dichloromethane was the virtual solvent selected based on its intermediate dielectric and the many moderately polar (some ionic) complexes targeted here. Solvation is expected to have significant energetic effects given the differing polarities of the various ligated metal species. Some optimizations were also run using the OPBE functional, which typically gave qualitatively similar results on the energy ordering of the LM(N_2O) spin states (see SI). In a few cases tested, *e.g.* (*N*-3Pyr)M(N_2O), M = V, Fe, the G_{solv} values from B3LYP/D3/SMD (6-31G(d)/LANL2DZ basis sets) and M06/SMD[49] (6-311+G(d,p)/SDD basis sets; no explicit dispersion) were compared and gave similar values (±2 kcal mol^{-1}) of binding affinities (SI). Hence, for uniformity and computational economy the B3LYP/D3/SMD (6-31G(d)/LANL2DZ) method was employed across all species. Transition states were found by relaxed scans of the M–O or N–O bonds, followed by a TS Berny optimization[50] (showing one imaginary

frequency along the reaction coordinate) and confirmed with IRC calculations in both the forward and reverse directions. Orbital analysis was carried out using the canonical orbitals from the B3LYP optimizations or the intrinsic bonding orbitals (IBOs).[51] The energy profile graphs were created using EveRplot.[52]

Results and discussion

Candidate complexes (complexants) for N_2O binding and O-transfer

A large set of potential N_2O-complexants/activators was selected for structural and energetic analysis with the several considerations in mind (Fig. 6). A small set of complexants, LM, was selected that are experimentally known to coordinate or react with N_2O for structural and energy-benchmarking to support the validity of the computational methods employed; these include (*N*-3Pyr)V (**1a**), $[(CF_3O)_4Al]Cu$ (**6**) and $(NH_3)_5Ru^{2+}$ (**7**). Since we are especially interested in identifying potential activators among the earth-abundant transition metals, we have focused on coordinatively unsaturated, reducing first row transition metals- Fe(II), Mn(II), Cr(II) and Cu(I)- with common supporting ligand types. Many of these metal centers have shown ability to coordinate or react with small unsaturated substrates (*e.g.* CO, ethylene, O_2, RN_3, N_2O) and the corresponding oxido-metal (LMO) species resulting from O-transfer are known, and some have demonstrated oxidizing ability.[53] Precious, second row LRu(II,III) species are also included for reference in this study because of their experimental precedents of N_2O complexation, activation and catalysis.[16,19–21,31,36] The ligand and coordination geometries include: tricoordinate *N*,*N*,*N*-(tris)pyrazolylborate/methane (TPB, TPM), tetracoordinate planar N_4-donors-porphyrin (POR), dipyrolyl-diimine (DPDI) and N_2O_2-donor-salen; 4-coordinate pyramidal ligands, *e.g. N-3Pyr* and 5-coordinate *N-4Py* and known derivatives with monodentate CN^- and NH_3 ligands. Many of the first-row metal derivatives of Fe(II), Mn(II), and Cr(II) are known or expected to be mid/high-spin species in their ground states.[54] Together the diversity of metal and ligand types selected will provide a broad assessment of the effects of metal, oxidation and spin states on the energetics of N_2O coordination and O-transfer to the metal.

Structural comparison of computed and experimental N_2O-complexes

In order to establish the reliability of the B3LYP methodology for predicting the structures of N_2O–metal complexes, we compared the X-ray structures of the experimental $[N\text{-}(Ar\text{-}Pyr)_3]V$ (N_2O) and copper–N_2O complexes (not shown) with the DFT-optimized structures of the ligand-truncated models (*N*-3Pyr)V (η^1-N_2O) (**1a**)[31c] and $[Al(OCF_3)_4]Cu(\eta^1\text{-}N_2O)$ (**6**) (Fig. 7).[31b] For both optimized structures the same experimentally observed linear η^1-N bonding mode was found; the calculated bond lengths and angles also were in very good agreement with the X-ray metrics (<±5%). We note also that the bond lengths within the N_2O unit are virtually unchanged upon coordination for these LV and LCu complexes, *cf.* Fig. 7 with free N_2O:[55] N–N 1.13 Å, N–O 1.18 Å, N–N–O 180°. This suggests rather little electronic perturbation to the N_2O unit upon coordination to these metal centers. The linear metal–N_2O geometry is also predicted for the low-spin Fe(II) derivatives evaluated, *e.g.* for $Fe(CN)_5(N_2O)^{3-}$ (**8**-N_2O, Fig. 7) and Fe(*N*-4Py)$(N_2O)^{2+}$ (**3**-N_2O) (SI). However, the more common mid/high spin iron(II) derivatives[54] that are investigated here typically optimized to a bent M–N_2O arrangement, *e.g.* Fe(POR)$(N_2O)^{t,qn}$ (**9**-N_2O) (Fig. 7) and (*N*-3Pyr)Fe($\underline{N}_2O)^{qn}$ (**1b**-N_2O, SI). A stronger metal–N_2O interaction in the linear LM–N_2O bonding mode is suggested by the considerably shorter Fe–N bond and longer N–O bond in the N_2O-adducts of complexants **3** and **8** compared to the angular **9**.

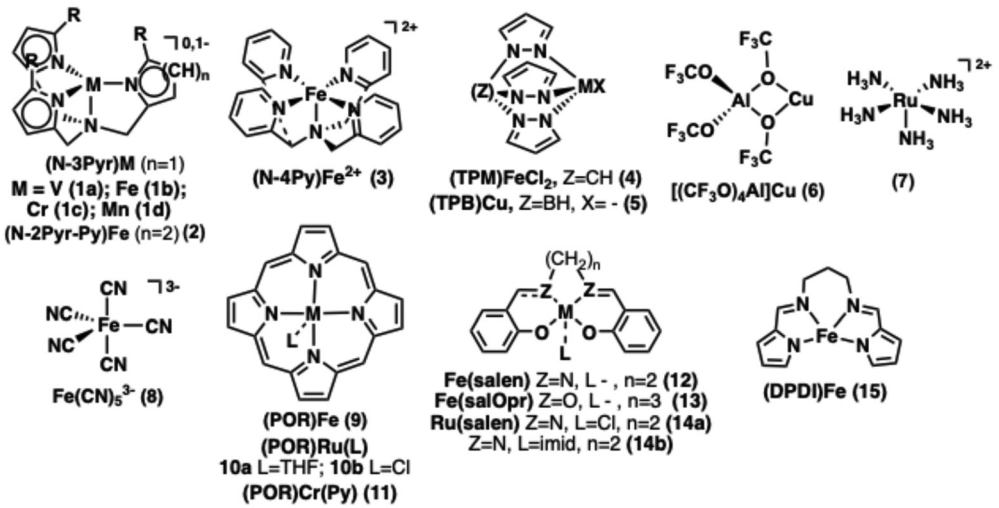

Fig. 6 Metal complexants evaluated for N_2O coordination and activation.

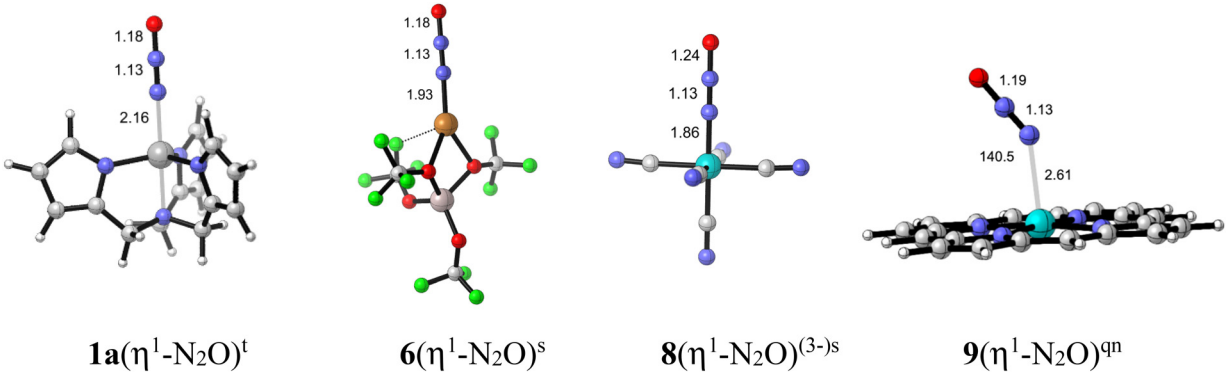

Fig. 7 B3LYP-optimized structures of η^1-N-bonded LM$(N_2O)^x$: (*N*-3Pyr)V$(\eta^1$-$N_2O)^t$, [$(CF_3O)_4$Al]Cu$(\eta^1$-$N_2O)^s$, $(CN)_5$Fe$(\eta^1$-$N_2O)^{(3-)s}$, (POR)Fe$(\eta^1$-$N_2O)^{qn}$; x = spin state, s = singlet, d = doublet, t = triplet, q = quartet, qn = quintet; atom colors: C = grey, H = white, blue = N, red = O, F = green, Al = pink, V = dark grey, Cu = bronze, Fe = turquoise.

The experimentally unknown O-bonding mode was also computationally evaluated for its geometrical and bonding features. This matter is of fundamental and practical importance because the most viable pathways for N–O cleavage likely involve LM–O–N_2 coordination. All the representative examples shown in Fig. 8 illustrate the favored bent arrangement of the M–O–N_2 unit (the N–N–O moiety remaining linear). As is the case with many of the N-bound complexes, the calculated metrics of the M–O–N_2 bound species show little O–N or N–N bond lengthening and the same linear N_2O geometry as in unbound N_2O; this indicates a small electronic perturbation to the coordinated N_2O for most, but not all, of the complexants investigated here.

To better understand the principal M–N_2O bonding components of the η^1-bonding modes the frontier bonding orbitals of representative complexes were examined. A canonical FMO for the linear $(CN)_5$Fe$(\eta^1$-$N_2O)^{3-}$ (**8**-N_2O) shows classical Fe–N_2O dπ–pπ* back-bonding (Fig. 9) with N–N π and O–N π* character. The optimized structure of **8**-N_2O^s (Fig. 7) shows a somewhat lengthened N–O bond (1.24 Å) relative to free N_2O (1.18 Å), probably reflecting substantial Fe–ON_2 electron density transfer, and decreased N–O bond order. The analogous, lower energy FMO for O-bound (*N*-3Pyr)V$(\eta^1$-$ON_2)$ (Fig. 9) has a smaller V d-orbital contribution, which could indicate lesser M–L back-bonding and shorter N–O distance (1.21 Å) relative to N-bonded 7-N_2O.

In contrast, both N- and O-bound linkage isomers of (*N*-3Pyr)Cr$(N_2O)^-$ (**1c**-$\underline{N}_2O$ and **1c**-$\underline{O}N_2$) exhibit acutely bent N–N–O fragments in both the N-bound and O-bound modes and a substantially elongated N–O bond relative to free N_2O (Fig. 10): Cr–N_2O 1.24 Å, Cr–ON_2 1.37 Å, free N_2O 1.19 Å; and a slightly longer N–N: Cr–N_2O 1.21 Å, Cr–ON_2 1.18 Å, free N_2O 1.13 Å. The bending of the N_2O unit may be the result of substantially greater Cr–X back-bonding relative to Fe(II). For the Cr-species the coordinated N_2O unit is essentially reduced, being electronically similar to the N_2O anion.[56] This species has a similar bent geometry with elongated N–O and N–N bonds relative to free N_2O. This view is also supported by the APT charges calculated for (*N*-3Pyr)Cr–O–N_2^-: Cr +1.86, O −0.71, N(1) +0.30, N(2) −0.27 (net −0.68e$^-$) *vs.* free N_2O: N(1) −0.31, N(2) +0.82, O −0.50. Significant electron spin density also resides in the coordinated N_2O unit: Cr 3.13, N(1) 0.14, N(2) 0.41, O 0.30 (though primarily local on Cr). The other high spin M–O–N_2 complexes show electron spin density located primarily on the metal and relatively little on the N_2O unit; *e.g.* in (*N*-3Pyr)V–O–N_2: V 2.06, N(1) −0.07, N(2) 0.08, O 0.06.

Although there are no structurally proven examples of bimetallic N_2O complexes, at least one such species has been

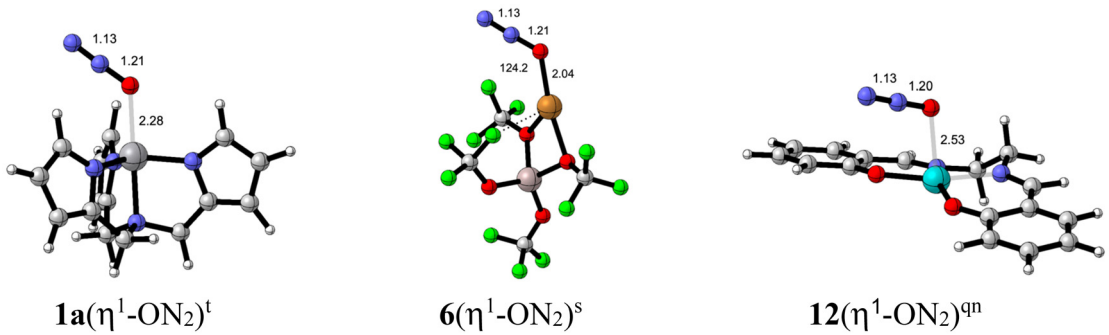

Fig. 8 DFT-optimized structures of O-bonded LM$(\eta^1$-$\underline{O}N_2)$. (*N*-3Pyr)V$(\eta^1$-$ON_2)$, [$(CF_3O)_4$Al]Cu$(\eta^1$-$ON_2)$, (salen)Fe$(\eta^1$-$ON_2)^{qn}$; free N_2O: N–N 1.13 Å, O–N 1.18 Å, N–N–O 180°.

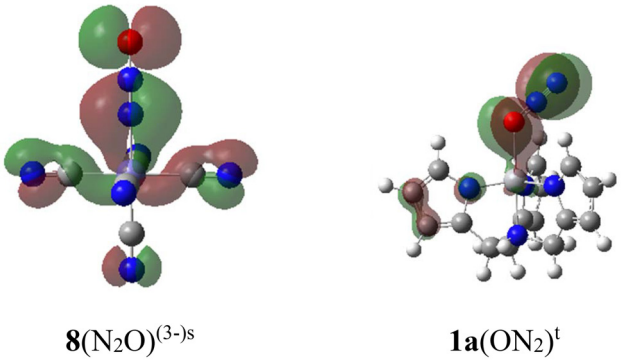

Fig. 9 HOMO-3 for $Fe(CN)_5(\eta^1\text{-}N_2O)^{3-}$ (left); HOMO-7 for (*N*-3Pyr)V(η^1-ON_2) (right) showing metal–(N_2O) π-(back) bonding contributions.

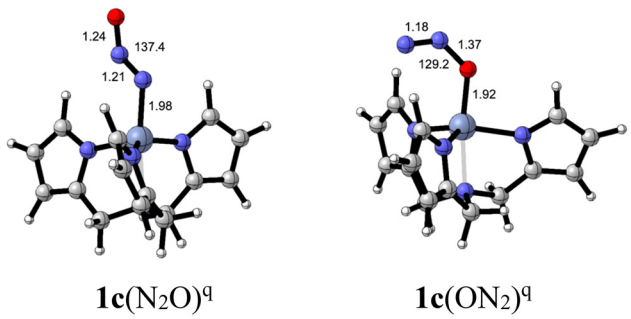

Fig. 10 Optimized structures of "abnormal" bent (*N*-3Pyr)Cr($\underline{N}_2O$)$^-$ and (*N*-3Pyr)Cr($\underline{O}N_2$)$^-$.

partially characterized[57] and others have been implicated in kinetics[34] and computational[8] studies of metal-promoted reactions of N_2O. Related non-metal bifunctional derivatives are represented in the frustrated Lewis pair (FLP) adducts of N_2O, $R_3P\text{-}N_2O\text{-}BX_3$.[29b,c] Accordingly, the structures and energetic viability of forming N_2O-bridged bimetallics was assessed for a set of metal complexants, specifically $Fe(POR)^{qn}$ (**9**), $Fe(salen)^{qn}$ (**12**), $Fe(DPDI)^t$ (**15**), $Cu(TPB)^s$ (**5**), $Ru(salen)(im)^s$ (**14b**) and $Ru(salen)Cl^d$ (**14a**) (Fig. 11). We were able to identify and optimize two types of structures- one with a linear bridging N_2O unit, generally of lower energy, and one with a distinctly bent N_2O-unit of higher energy. For the linear bimetallic iron derivatives, *e.g.* (salen)Fe-N_2O-Fe(salen) (**12**-N_2O-**12**), the N–N and N–O bond lengths are little changed from free N_2O and the Fe–O (3.5 Å) and Fe–N (3.1 Å) distances are long, more typical of non-covalent encounter complexes held by dispersion/London electrostatic forces.[58] Linear (TPB)Cu-N_2O-Cu(TPB) (**5**-N_2O-**5**) shows more typical Cu–N,O bond lengths and little changed N–N and N–O distances relative to free N_2O. The linear (salen)(im)Ru-N_2O-Ru(salen)(im) species (**14b**-N_2O-**14**b) exhibits typical covalent Ru-N,O bond lengths, and somewhat longer N–O distances, suggesting appreciable Ru-O,N back-bonding. For the *bent* bimetallic complexes, *e.g.* (salen)Fe-N_2O-Fe(salen) (**12**-N_2O-**12**) one sees marked bending of the N_2O unit and lengthening of the N–N and N–O bonds: N–N 1.19 Å, N–O 1.37 Å, N–N–O 125° relative to its linear counterpart (Fig. 11). The shorter Fe–N and Fe–O distances imply a stronger M–N_2O interaction and perturbation of the N_2O electronic character. One finds similar features for the corresponding bent (DPDI)Fe derivative **15**-N_2O-**15**. Metrics of the bent N_2O mode in these examples are indicative of considerable structural and electronic perturbation of the coordinated N_2O unit, comparable to those of the N_2O anion.[56] This suggests considerable electron transfer from iron to the N_2O-unit, *i.e.* reduction, in the bent bimetallics and is supported by the calculated APT charges, *e.g.* for *bent* **12**-N_2O-**12**, Fe(+1.70)–O(−0.77) and Fe(+0.51)–N1(0.29) *vs.* for *linear* **12**-N_2O-**12**, Fe(+0.80)–O(−0.44) and Fe(+0.80)–N1(−0.29).

Energetics of N_2O binding

The free energy of association ΔG_a between N_2O and the metal complexants was calculated by determining the free energy values for each species in its optimized ground spin state for the reaction, LM + N_2O → LM(N_2O). For a more accurate comparison to typical experimental solution data, corrections to the free energy *in vacuo* were made for dispersion (D3) and solvation (SMD). The free energy results for the set of experimentally investigated N_2O complexes, Group I, are summarized in Table 1. The dispersion correction generally lowered the ΔG_a (increases K_a), while the solvation correction typically raised ΔG_a, which tended to offset. In cases that were compared, the free energies of binding, ΔG_a, with B3LYP-D3/SMD or M06/SDD-6-311+G(d,p)/SMD were quantitatively similar, ±2 kcal.

Each of the Group I examples of experimentally implicated N_2O complexes shows a thermodynamically favorable (exergonic) free energy of association ΔG_a (binding affinity) in the solution phase, which qualitatively agrees with the demonstrated isolability/stability of these compounds. For the models of the isolated/X-rayed vanadium- and copper-complexes, **1a**-N_2O and **5**-N_2O, modest to substantial binding free energies (−1.5, −7.0 kcal mol^{-1}) are calculated when both dispersion and solvation effects (in CH_2Cl_2) were factored in; corresponding K_a values would be on the order of 10^2–10^{10}. Unfortunately, the experimental equilibrium constants for these complexes have not been measured. For the (POR)Ru(THF)/N_2O system (**10a**-N_2O) a very favorable binding affinity (ΔG_a −7.3 kcal mol^{-1}) is estimated. We note that a transient (undetected) N_2O adduct is presumed in the room temperature reaction between (TMP)Ru to form (TMP)RuO_2.[36] In the three examples of isolable N_2O complexes, the experimentally established N-bound linkage isomer was strongly favored by 7–25 kcal mol^{-1} over the O-bound form. A recent DFT analysis of $(NH_3)_5Ru(N_2O)^{2+}$ (7-N_2O) reported the same structures and selectivity ($\Delta G_{O/N}$ 6.9 kcal) in favor of the N-bound mode as here.[59] In the case of the only N_2O association equilibria experimentally studied, the $(NH_3)_5Ru(H_2O)^{2+}/N_2O$ system,[31a] we calculated a value for ΔG_a of −2.4 kcal mol^{-1} for the aqueous phase reaction LRu(H_2O) + N_2O → LRu($\underline{N}_2O$) + H_2O, corresponding to a K_a = 57. This can be compared to the experimentally determined K = 7 (ΔG *ca.* −1.1 kcal mol^{-1}). The

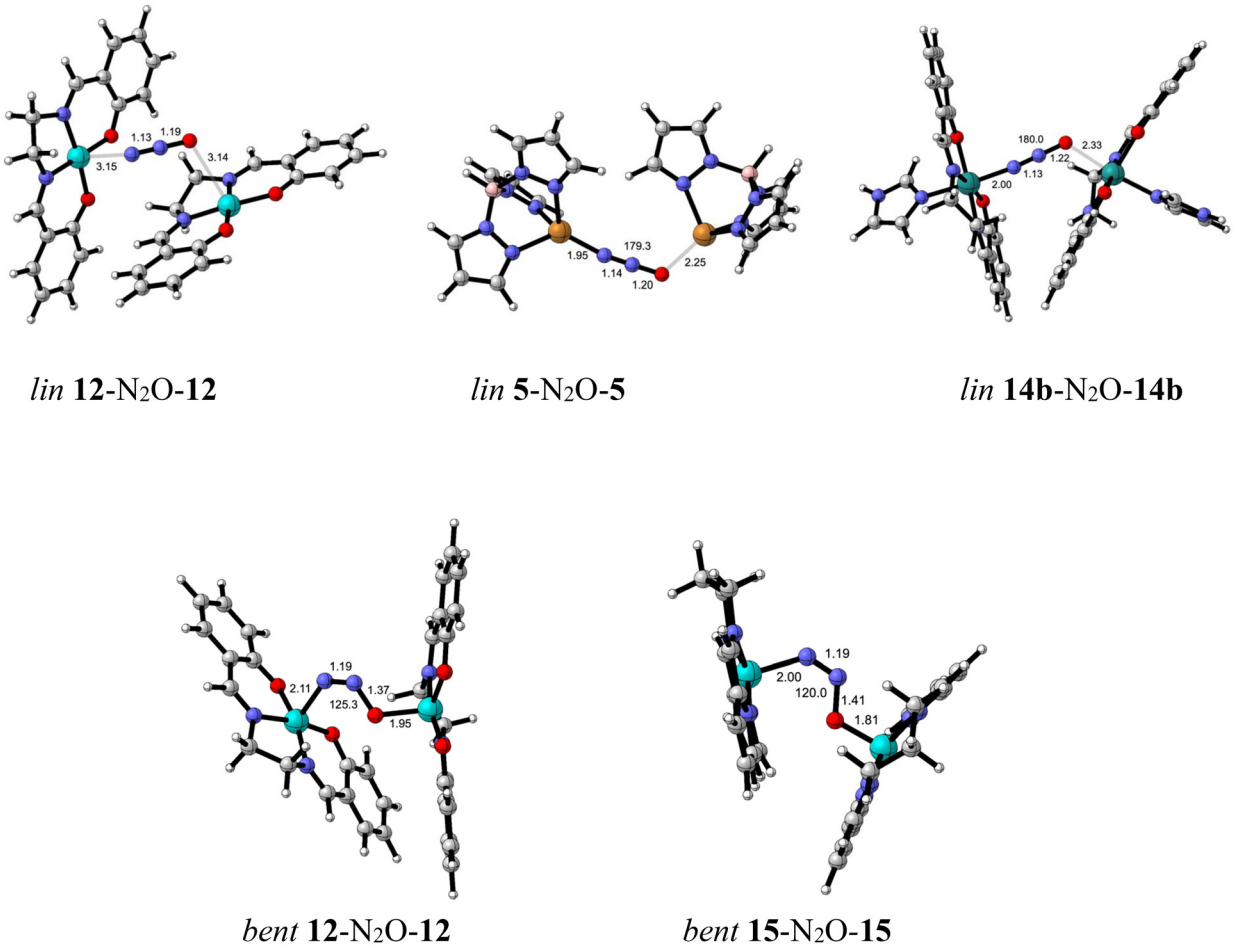

Fig. 11 Top: optimized μ-linear structures of (salen)Fe-N_2O-Fe(salen)^{qn}, (TPB)Cu-N_2O-Cu(TPB)^{s} and (imid)(salen)Ru-N_2O-Ru(salen)(imid)^{s}. Bottom: optimized μ-bent structures of (salen)Fe-N_2O-Fe(salen)^{qn} and (DPDI)Fe-N_2O-Fe(DPDI)^{qn}.

quantitative discrepancy between theory and experiment may be the composite result of several factors: (1) the neglect of the counter anion in the calculation; (2) the inaccuracy of the DFT functional or the solvation model for this 2+ complexed ion, where specific H-bonding could be significant between the ligated NH_3, N_2O and the solvent H_2O; and (3) the inaccuracy of the experimental measurement. Nonetheless, semi-quantitative agreement was found between calculation and experiment for the N_2O binding affinities among these experimentally established LM–N_2O systems.

For the Group II iron-based potential N_2O-complexants (Table 1) several significant features of the binding free energy, ΔG_a, were discovered. First, with few exceptions the ΔG_a values for the 4-coordinate complexants are slightly to considerably unfavorable, in the range of +1 to 6 kcal mol^{-1}. There is some variation in ΔG_a among the planar ligated iron species, with little difference among the N_4- and N_2O_2-ligated species, FeL = POR (**9**), salen (**12**), and DPDI (**15**), but lower affinity for the expectedly weaker donating O_4-ligand, (salOpr)Fe (**13**). For the 4-coordinate pyramidal fragments, M(*N*-3Pyr) (**1b**) and *N*-2Pyr-Py (**2**), the binding free energies ΔG_a are comparable to the planar ones, which at first seems inconsistent with the experimental O-transfer reactivity of the Fe-derivative **1b** (R = Ar) with N_2O reported by Chang's group.[60] This issue is addressed subsequently with the Group III results of Table 1 and the energetics of the O-transfer activation energies (Table 2). An indication that the pyramidal *N*-3Pyr ligand can provide for favorable N_2O binding and activation is evidenced by the proven (*N*-3Pyr)V(N_2O) complex (**1a**-N_2O)[31c] and the virtual Mn- and Cr-N_2O derivatives **1d**, **1c** that we present later. Among the 5-coordinate iron(II) complexants (L = *N*-4Py, **3** and $Fe(CN)_5^{3-}$, **8**) there is some variation in the calculated ΔG_a values, but N_2O-binding appears to be somewhat more favorable with these species, ΔG_a(av) = −0.4 (vac), +1.7 (CH_2Cl_2), relative to the planar derivatives. The strongest predicted iron(II)–N_2O complexant is 5-coordinate $[(N\text{-}4Py)Fe]^{2+}$ (**3**), ΔG_a < −6.3/−6.8 kcal mol^{-1} (vac/CH_2Cl_2). As to the origin of this expected affinity, we note the differences in both charge (2+), coordination number (5) and favored spin state (singlet) *vis a vis* the other 4- and 5-coordinate iron(II) species, which usually have triplet- or quintet ground states.[54] Based on the set of iron(II) complexants considered here, 5-coordinate, square pyramidal, low spin

Table 1 Computed thermodynamics of nitrous oxide association with metal complexants

$LM + N_2O \rightarrow LM(\underline{N}_2O)$ ΔG_a

LL′M	Ground spin state[a] LM/LM (N_2O)	$\Delta G_{N/O(rel)}$[b] (kcal mol^{-1})	$\Delta G_{a(vac)}$[c] (kcal mol^{-1})	$\Delta G_{a(D,CH2Cl2)}$[d] (kcal mol^{-1})
Group I				
(*N*-3Pyr)V (**1a**)	T/T	7.0	−2.9	−1.4
$(NH_3)_5(H_2O)Ru^{2+}$ (**7**)	S/S	7.7	9.0	−2.4[x]
(POR)(THF)Ru (**10**)	S/S	10.3	−3.9	−7.3
$[(CF_3O)_4Al]Cu$ (**6**)	S/S	25.7	−11.9	−7.0
Group II (M = Fe)				
(POR)Fe (**9**)	Q/Q	0.3	2.1	1.8
(DPDI)Fe (**15**)	T,T	−0.1	3.0	1.2
(salen)Fe (**12**)	Qn/Qn	0.2	3.6	2.9
(salOpr)Fe (**13**)	Qn/Qn	0.1	6.2	6.5
$(N\text{-}3Pyr)Fe^{1-}$ (**1b**)	Qn/Qn	—[e]	4.5	4.1
(*N*-2Pyr-Py)Fe (**2**)	Qn/Qn	−0.1	−1.1	4.7
$(TPM)Cl_2Fe$ (**4**)	T/S	0.4	0.3	3.2
$(N\text{-}4Py)Fe^{2+}$ (**3**)	S/S	6.7	−6.3	−6.8
$(CN)_5Fe^{3-}$ (**8**)	T/S	—[e]	0.6	3.4[f]
Group III (M ≠ Fe)				
(salen)(imid) Ru (**14a**)	S/S	4.7	−3.7	−1.5
(salen)ClRu (**14b**)	D/D	0.9	3.6	1.4
(POR)ClRu (**10a**)	D/D	0.8	6.6	10.1
(TPB)Cu (**5**)	S/S	5.3	−3.0	−1.5
(POR)(Py)Cr (**11a**)	T/T	2.3	−12.0	−14.5
$(N\text{-}3Pyr)Mn^-$ (**1d**)	Sx/Sx	0.1	4.6	5.2
$(N\text{-}3Pyr)Cr^-$ (**1c**)	Q/Q	−3.6	−1.7	−1.4

[a] Spin state multiplicities: S = singlet, T = triplet, Q = quartet, Qn = quintet, Sx = sextet Solvent = H_2O. [b] N/O selectivity, $\Delta G_{N/O} = G_{LM(\underline{O}\text{–}N2)} - G_{LM(\underline{N}2O)}$ [c] $\Delta G_{a(vac)} = G_{LM(\underline{N}2O)} - G_{LM} + G_{N2O}$ [d] $\Delta G_{a(D,CH2Cl2)} = \Delta G_{a(vac)}$ corrected for dispersion (D3) and solvation (SMD-CH_2Cl_2) [e] Optimization of $LM(\eta^1\text{-}\underline{O}N_2)$ did not converge [f] SMD solvent = H_2O

complexes should bind most favorably to N_2O. Another interesting feature of the Group II data in Table 1 is the much smaller difference in binding free energy between the N- and O-bound adducts of the high spin species, $\Delta G_{N/O}$ ±2 kcal, when compared to the known/implicated (Group I) and low spin N_2O complexes, $\Delta G_{N/O}$ 6–25 kcal favoring the N-bound isomers. This smaller N/O-binding selectivity among the high spin adducts also parallels their similar and longer metal-O,-N bond lengths and bent geometries compared to the low spin linear M–N_2O adducts, *e.g.* in Fig. 7 and 8.

The binding affinity data for a set of similarly ligated, non-ferrous metal complexants (Group III) are also provided in Table 1. For the (salen)Ru(imid) relative **14b** in its most stable singlet state, the ΔG_a for N_2O is exergonic, −3.7 (vac) and −1.5 (CH_2Cl_2) kcal mol^{-1}, in contrast to that of its high spin, iron relative (ΔG_a =+3.6 kcal mol^{-1}). Higher oxidation state d^5-(L)Ru (III)Cl derivatives (*e.g.* L = POR, salen) were found to have lower N_2O affinities, ΔG_a for **13b**-N_2O +3.6 (vac), +1.4 (D, solv) kcal mol^{-1}; for **9a**-N_2O +6.6 (vac) and +10.1 (CH_2Cl_2) kcal mol^{-1}. The oxidation state effect on binding affinity illustrated here is consistent with the weak σ-donor, moderate π-acceptor character of N_2O and the more electron-accepting, weaker back-bonding character of Ru(III) *vs.* Ru(II). The last set of Group III complexants include derivatives of non-precious Mn, Cr and Cu. The (TPB)Cu singlet species (**5**) is calculated to form a relatively stable N-bound adduct, ΔG_a = −3.0 (vac) and −1.5 (CH_2Cl_2) kcal mol^{-1}, making it a good prospect for reactivity studies with N_2O. We note the proven ability of (TPB)Cu derivatives to bind weakly donating/pi-accepting substrates (CO, acetylene, ethylene).[61] Our calculations suggest that N_2O-binding to (TPB)Cu (**5**) would be less favorable energetically than for the isolated $[(R_FO)_4Al]Cu\text{-}N_2O$ (**6**).[31b] The (POR)(Py)Cr (N_2O) species (**11**-N_2O), which is predicted to be a GS triplet, is calculated to have the strongest binding affinity to N_2O among the monometallic species considered here, ΔG_a = −12.0 (vac) and −14.5 kcal mol^{-1} in CH_2Cl_2.

An indication that N_2O binding and activation may be facilitated more generally by low valent complexes of the *N-3Pyr* ligand is supported initially by our computational results for the M = V(III) (**1a**-N_2O) and Fe(II) (**1b**-N_2O) models of the complexes that react with N_2O at room temperature.[31c,60] The computational picture for the $(N\text{-}3Pyr)Fe^-/N_2O$ interaction is complicated; the more stable quintet fragment doesn't show high affinity for N-binding, ΔG_a +4 kcal mol^{-1}, while binding to the less stable triplet is very favorable, −6.4 kcal mol^{-1} (for the N-bound isomer). Energy scans on the quintet $LFe\cdots ON_2$ surface revealed no distinct LFe–O–N_2 minimum or TS (more later). N- and O-bound N_2O adducts could be optimized for the corresponding $(N\text{-}3Pyr)Mn/N_2O$ system (**1d**-N_2O) in the most stable high spin (sextet) state but, again, the binding equilibrium with N_2O is unfavorable. As noted earlier, $(N\text{-}3Py)Cr(N_2O)^t$ (**1c**-N_2O) optimized to the unusual bent/bent coordination modes for both the N-

Table 2 Energetics of O-transfer *via* mono and bimetallic N_2O complexes[a]

Monometallic : $LM + N_2O - (\Delta G_a) \rightarrow LM - O - N_2 \cdots (TS, \Delta G^{*}_{O-N}) \rightarrow LM{=}O + N_2\ \Delta G_{OT}$

Bimetallic : $LM + N_2O - (\Delta G_a) \rightarrow LM - N_2O - ML \cdots (TS, \Delta G^{*}_{O-N}) \rightarrow LM, O + LM + N_2\ \Delta G_{OT}$

LM fragment[b]	ΔG_a LM(ON$_2$)(ML) (kcal mol^{-1})	ΔG^{*}_{O-N} (kcal mol^{-1})	ΔG^{*}_{span} (kcal mol^{-1})	ΔG_{OT} (kcal mol^{-1})
Monometallic				
Fe(POR)^{qn,t} (**9**)	1.8	25.4	27.2	−24.1
Fe(DPDI)^{t,t} (**15**)	1.2	32.4	33.6	−21.0
Fe(*N*-4Pyr)$^{(2+)s,t}$ (**3**)	2.0	27.2	29.2	−36.5
Fe(salen)^{qn,t} (**12**)	2.2	31.8	34.0	−19.1
Fe(*N*-3Pyr)$^{(-)qn,qn}$ (**1b**)	—[c]	—[c]	26.0	−29.9
Fe(*N*-2Pyr-Py)^{qn,qn} (**2**)	4.7	23.0	27.7	−27.1
Fe(TPM)Cl$_2^{t,t}$ (**4**)	2.0	31.7	33.7	−18.4
V(*N*-3Pyr)$^{(-)t,s}$ (**1a**)	5.4	13.6[d]	19.0[e]	−114.9
Mn(*N*-3Pyr)$^{(-)sx,q}$ (**1d**)	4.7	22[d]	26.7[e]	−67.2
Cr(*N*-3Pyr)$^{(-)qn,t}$ (**1c**)	−1.7	2.6	0.9	−67.1
Cr(POR)(Py)^{t,t} (**11**)	3.4	5.6	9.0	−62.8
Cu(TPB)^{s,t} (**5**)	4.2	33.6	37.8	−4.8
Ru(POR)(THF)^{s,s} (**10**)	3.0	16.5	19.5	−47.4
Ru(salen)(imid)^{s,s} (**13a**)	3.3	17.3	20.6	−43.6
Ru(salen)Cl^{d,d} (**13b**)	3.5	21.2	24.7	−29.5
LM–N_2O–ML Bimetallic			ΔG^{*}_{span} (bimet. adv.)[f]	
Fe(POR)^{qn,t} (**9**)	22.0 (μ-bent)	1.7	23.7 (−3.5)	−24.1
Fe(DPDI)^{qn,t} (**15**)	20.1 (μ-bent)	2.2	22.3 (−11.3)	−21.0
Fe(salen)^{qn,t} (**12**)	3.2 (μ-linear)	22.6	25.8 (−8.2)	−19.1
	21.7 (μ-bent)	4.1	25.8 (−8.2)	−19.1
Cu(TPB)^{s,t} (**5**)	2.0 (μ-linear)	18.0	20.0 (−15.6)	−4.8
Ru(salen)(im)^{s,s} (**14a**)	−2.6 (μ-linear)	4.7	2.1 (−18.5)	−43.6
Ru(salen)Cl^{d,t} (**14b**)	11.8 (μ-bent)	−0.5	11.8 (−12.9)	−29.5

[a] B3LYP/D3/SMD-CH_2Cl_2, T = 298 K. [b] Superscripts indicate ground spin states of LM(ON$_2$) or LM–N_2O–ML and LMO respectively; spin state multiplicities: s = singlet, t = triplet, q = quartet, qn = quintet, sx = sextet. [c] O-bound isomer did not optimize. [d] Estimated energy barrier from two-dimensional M–O/N–O scans corrected for dispersion and solvation. [e] ΔG^{*}_{span} = free energy change from lowest energy intermediate to transition state. [f] Bimetallic advantage = ΔG^{*}_{span} for LM(O − N_2) − ΔG^{*}_{span} for LM--N_2O--ML.

and O-bound species (Fig. 9). Moreover, both showed mildly exergonic binding to N_2O and with little expected N/O-binding selectivity as often seen for the high spin complexants. This system provides a unique example of likely favorable N_2O-binding with little expected N/O-selectivity. Could an O-bound N_2O complex be produced selectively in this case? Our computational results, combined with experimental support from the N_2O interactions with (*N*-3Pyr)-V [31c] and -Fe[60] suggest a special ability of low valent M(*N*-3Pyr) species to react with and transform N_2O (*vide infra*). Considering the computational results summarized with this set of ligands, the following metal-dependent binding affinity order is predicted based on ΔG_a: LCr(II) > LRu(II) > LV(III) > LFe(II) ≈ LMn(II) ≈ LCu(I). This ordering of binding affinity correlates with M–N_2O or M–ON_2 bond strength and roughly parallels the oxidation potentials and electronegativity trends among the free metal ions. Since N_2O is a weak σ-donor/strong π-acceptor, stronger binding will result with stronger pi-donating (back-bonding) and weak acceptor complexants – *i.e.* earlier TMs in lower oxidation states, *e.g.* Cr(II), V(III) > Fe(II), Mn(II), Cu(I) and second row > first row transition metal moieties, *e.g.* Ru(II) > Fe(II).

O-transfer to metal

To facilitate N–O scission one presumes that a potential monometallic complexant, LM, would bind to N_2O *via* the O-atom, producing LM(η^1-O$\underline{N}_2$). From the O-bound complex, O-transfer to the metal would proceed *via* O–N bond-breaking (and O–M bond-making) to yield the O=ML species with N_2 dissociation. Transition states (TSs) for O–N scission for each of the selected complexants (in their ground spin states) were located by 1D or 2D ModRedundant scans along the O–N and/or O–M coordinates followed by Berny TS optimization. A set of representative TSs located by this approach is displayed in Fig. 12. Each of these species shows a bent O–N_2 unit with a considerably elongated O–N distance (1.26–1.57 Å) relative to its precursor N_2O complex (see *e.g.* Fig. 7) and to free N_2O. The TS structure for (*N*-3Pyr)Cr(O-N_2)$^{-}$* (Fig. 12) showed shorter Cr–O (1.90 Å) and longer O–N (1.57 Å) bond lengths compared to its precursor **1c**-ON_2; 1.92 Å, 1.37 Å; (Fig. 9), as expected for continuation of N–O scission *en route* to (*N*-3Pyr)CrO^{-} and N_2. The variable length of the cleaving N–O bonds in these TSs (Δ_{O-N} 0.30 Å) is substantial and not obviously correlated with the corresponding activation energies from the precursor LM–ON_2 complexes (*vide infra*). It is noteworthy that among these, two dihedral M–O···N–N conformations, *syn* and *anti*, are displayed.

Some insight into the electronic and bonding changes that occur in transforming the O-bound intermediates to their transition states is provided by analyzing the change in atomic charges and frontier molecular orbitals (FMO). As an example,

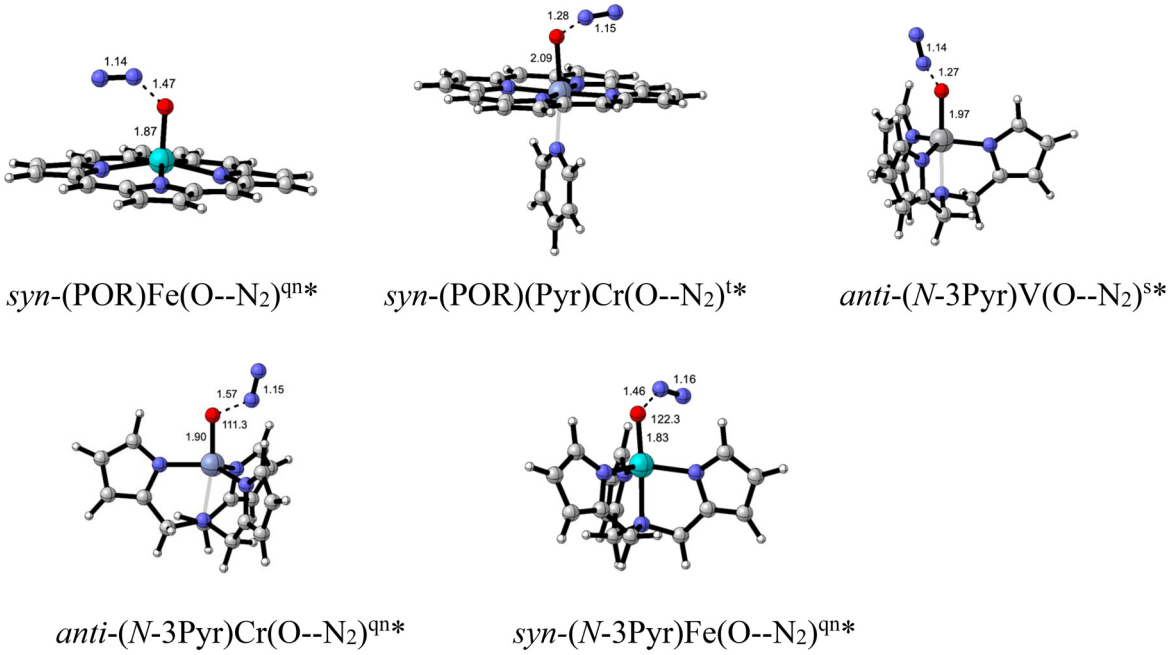

Fig. 12 Transition state structures for monometallic LM–O···N_2*.

for the (salen)Fe–ON_2 to (salen)Fe–O···N_2* transformation, the APT (Atomic Polar Tensor)[62] charge distribution within the Fe–O–N–N unit changes are: Fe +1.34 to +1.43, O +0.56 to −0.24, N1 +0.76 to −0.05, indicating partial iron oxidation and O- and N-reduction. Further conversion to the products, (salen)Fe=O^{qn} and N_2, show further redox changes: Fe +1.54 (oxidized), O −0.45 and N 0.0 (reduced). In Fig. 11 we show selected FMOs with important contributions to Fe–O–N–N bonding and their energies for the same conversion. For (salen)Fe(η^1-ON_2): SOMO-5 is weakly Fe–O π-bonding (π), O–N is π-antibonding (π*) and N–N is π, while SOMO-6 is Fe–O σ, O–N π* and N–N π. For (salen)Fe(η^1-O···N_2)*: SOMO−5 is Fe–O π, O–N π* and N–N π, while SOMO-8 is Fe–O σ, O–N π* and N–N π. The lower energy (stabilization) of these FMOs in the TS relative to the reactant LFe(ON_2) intermediate thus increases the Fe–O and N–N bond orders and decreases the O–N bond order. This is consistent with the electron flow suggested by the APT analysis and the bond-making/breaking represented in the simple valence bond picture of Fig. 13c. The valence electron pair model is an oversimplification, however, given the likely open shell electronic state of (**12**-ON_2) and most of the other iron(II) complexes.

The structural and energetic viability of bimetallic N_2O coordination and promotion of N–O cleavage was also evaluated. Among the several bimetallic N_2O-complexes optimized previously (Fig. 11 and Table 1), we located and optimized most of their transition state structures. Two representative examples are shown in Fig. 14. For both the salen-iron (**12**-N_2O-**12**) and the related ruthenium species (**14b**-N_2O-**14b**), one finds bent M–N_2O–M units and very long N–O distances indicative of advanced N–O bond-breaking in a very late transition state. Comparison of the iron bimetallic intermediate **12**-N_2O-**12** (Fig. 11) to the corresponding TS (Fig. 14) shows longer N–O distances (1.37 *vs.* 1.58 Å) and shorter N–N (1.19 *vs.* 1.15 Å) and Fe–O (1.95 *vs.* 1.88 Å) lengths in the TS, as expected for progress along the reaction coordinate to the products- LFe=O, LFe and N_2. Similar changes are found for the Ru-intermediate (**14b**-N_2O-**14b**) and TS (SI).

Energetics of O-transfer to mono-metallic species

Free energies for the optimized structures of intermediates and TSs for the O-transfer to LM are tabulated in Table 2 based on the pathway: LM–O–N_2 and LM–N_2O–ML to LM=O (+LM) + N_2. Key results and trends for the monometallic complexants are summarized first. For most of the mono-LFe(II) complexes the overall reaction free energy ΔG_{OT} is moderately to highly exergonic (−13 to −36 kcal/mole) and the affinity for O-binding is modest (ΔG_a +1–5 kcal mol^{-1}). The activation energies ΔG^*_{O-N} for O–N cleavage of LFe–O–N_2 generally are moderate to high, ranging from 23–32 kcal, with the corresponding energy span barriers, ΔG^*_{span} ,[63] (from LM + N_2O) being slightly higher, 25–34 kcal mol^{-1}. The pyramidal *N*-2Pyr-Py ligand confers a somewhat lower activation energy to its iron(II) complex **2**-ON_2 (23 kcal mol^{-1}) and a lower energy span barrier (27.7 kcal mol^{-1}) than do the various planar ligands. The consequences of the calculated energetics for these species are that generation of potentially reactive oxido-metal intermediates, LFe(IV)=O, should be practically viable at moderate to relatively high temperatures, *e.g.* 100–150 °C.[64]

The (*N*-3Pyr)M platform has two representatives, M = V and Fe, with experimentally demonstrated N_2O reactivity, the former providing an isolable (N-bound) complex[31c] and the latter deoxygenating N_2O readily.[60] Therefore, we sought to

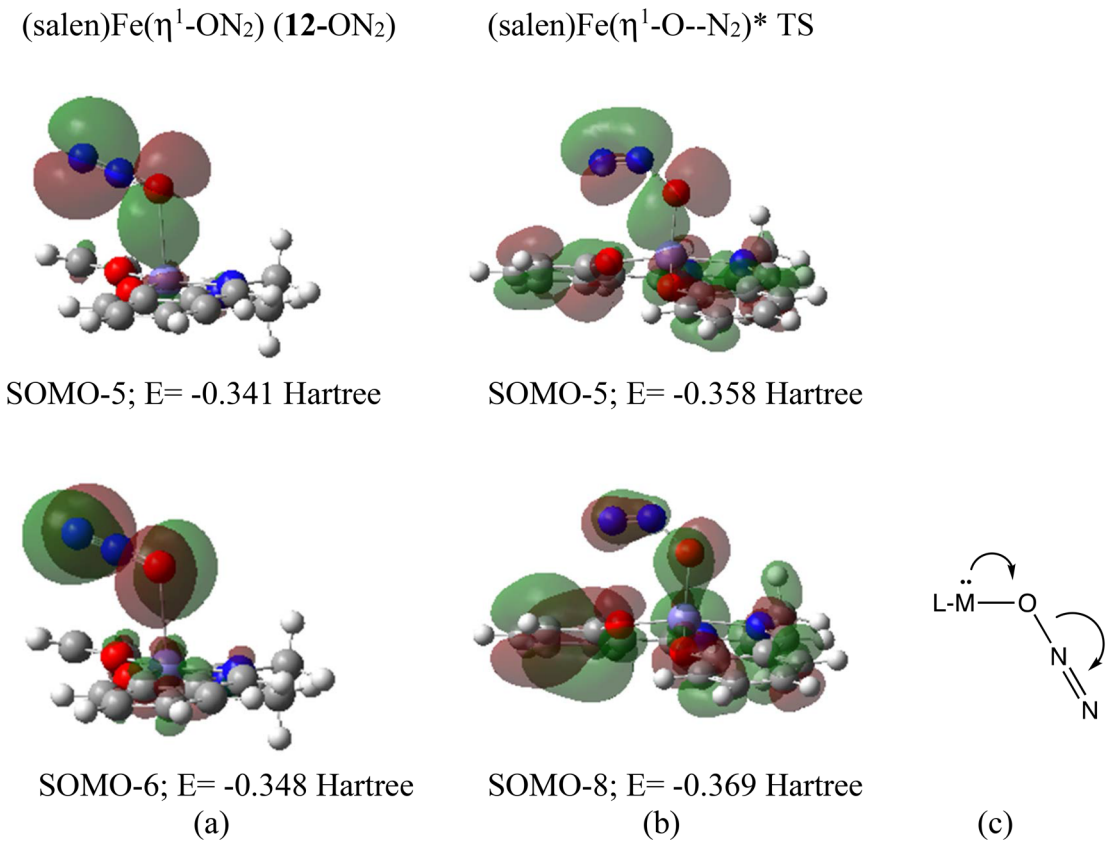

Fig. 13 Correlated FMOs involved in Fe–O–N_2 bonding and their relative energies (Hartree) for (a) (salen)Fe(O-N_2)^{qn}; (b) TS (salen)Fe(η^1-O···N_2)*; (c) the valence bond representation of electron flow during LMO···N_2 scission.

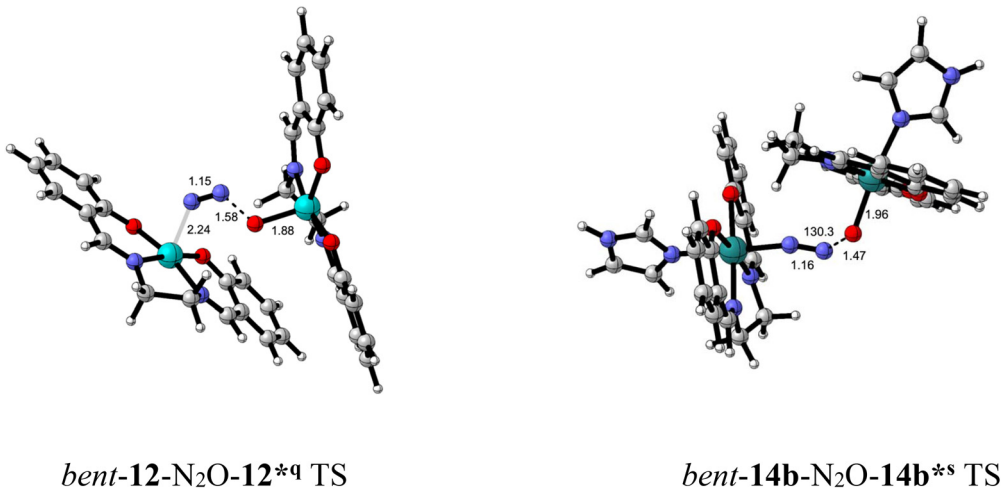

Fig. 14 Transition state structures for (salen)Fe-N_2O-Fe(salen)*^{qn} and (imid)(salen)Ru-N_2O-Ru(salen)(imid)*^{s}.

analyze these and two unknown congeners computationally, M = V (d^2), Cr (d^4), Mn (d^5) and Fe (d^6). The (*N*-3Pyr)M(O-N_2) complexes have large to huge calculated exergonicities for the O-transfer reaction to produce (*N*-3Pyr)M═O$^-$ (>−30 to −115 kcal, Table 2). B3LYP calculations predict that all but the (*N*-3Pyr)Fe derivatives change ground spin states (GSS) between the LM–ON_2 reactant and product LM═O: *i.e.* V, T/S; Cr, Q/T; Mn, Sext/Q. This set of complexes provided significant computational challenges to locate well-defined LM–O–N_2 intermediates and transition states, and complicated by these

spin-state changes.[65] The (*N*-3Pyr)Fe$^-$ complexant **1b** is the exception here as both LFe(O-N_2) and LFe=O are calculated as GS quintets. However, a discreet (N-3Pyr)Fe-ON_2^{qn} intermediate was not found, but a true TS on the quintet surface was located displaying typical features of the transforming M–O–N_2 unit, *i.e.* the bent linkage and elongated O–N distance (1.46 Å, Fig. 12). A moderate activation barrier, ΔG^*_{span} of 26.0 kcal mol^{-1} (from the unbound complexant + N_2O) is found, consistent with the experimentally observed facile reaction of [*N*-3(Mes-Pyr)]Fe$^-$ with N_2O.[60] The association of N_2O and O-transfer conversion process in this case appears to be essentially concerted. While N-binding of N_2O to the triplet V-derivative (**1a**) is exergonic (ΔG_a −1.4 kcal), consistent with its experimental isolation,[31c] O-binding is unfavorable (ΔG_a +5.4 kcal). The lowest energy pathway from the ground state triplet of (*N*-3Pyr)V(η^1-ON_2) (**1a**-ON_2) to the GS singlet of (*N*-3Pyr)VO (+N_2) is unclear. One dimensional and 2D scans along the V–O and O–N distances of (**1a**-ON_2)^t towards LVO^t increase in energy with a maximum at about 20–24 kcal and then descend toward the triplet product +N_2 without a verifiable TS (SI). A TS could be located on the singlet surface with a moderately large activation energy, $\Delta G^*_{OT} = 26$ kcal $\left(\Delta G^*_{span} = 27.4\,\text{kcal}\right)$, but given the extraordinary exergonicity overall to produce the singlet LVO species (>100 kcal mol^{-1}), it seems probable that as the triplet LV–O···N_2 maximum is approached there is spin crossover to the singlet surface as the energy plunges to the singlet product with N_2 dissociation. The O–N scission process for the hypothetical (*N*-3Pyr)Mn-ON_2^- formulated as a GS sextet, is similar to the vanadium relative, with unfavorable binding (ΔG_a +4.7 kcal). Like the LV(O-N_2) OT conversion, two-dimensional O–N and Mn–O coordinate scans from the (*N*-3Pyr)Mn-O-N_2^- sextet rose energetically through a maximum that did not optimize to a legitimate TS. The species at the spin crossover point to the quartet surface of the product, when compensated energetically with thermal/frequency, dispersion and solvent corrections, led to an approximate maximum with an estimated ΔG^*_{span} of a moderate 22 kcal mol^{-1}. In contrast, as noted earlier, the O-bound (*N*-3Pyr)Cr-ON_2 intermediate (**1c**-ON_2) could be optimized (Fig. 10) and showed a rare favorable binding energy for both the N- and O-bound isomers (ΔG_a −3.6, −1.7 kcal). From **1c**-ON_2 a true TS was located (Fig. 12) with a remarkably small activation energy ΔG^* = 2.6 kcal and a highly exergonic overall O-transfer energy (−67 kcal mol^{-1}). After mounting this negligible barrier, presumably spin crossover to the GS triplet of the product (*N*-3Pyr)Cr=O would occur. The Cr(II) complexant **1c** is thus predicted to readily deoxygenate N_2O to generate the potentially reactive (*N*-3Pyr)Cr(IV)(O)$^-$ species.[66] The other Cr(II) species (POR)(Py)Cr^t (**11**) is calculated to have modest affinity for O-bound N_2O (ΔG_a +3.4 kcal), but it too was found to have a low activation energy and energetic span barrier, 5.6 and 9.0 kcal mol^{-1} respectively for N–O scission *via* an early TS (Fig. 12). This low barrier prediction is in accord with the reported ambient deoxygenation reaction between N_2O and (TMP)Cr/N_2O.[67] These Cr(II) derivatives constitute attractive systems for further experimental reactivity studies with N_2O (and with oxidizable substrates). In contrast, the late first row metal complexant Cu(TPB)^s (**5**) was found to have a modest O-binding affinity for N_2O (ΔG_a +4 kcal mol^{-1}), a rather large activation energy ΔG^*_{N-O} of 33.6 kcal (ΔG^*_{span} 37.8 kcal), and a comparatively small exergonicity for the overall O-transfer reaction (ΔG_{OT} −4.6 kcal), probably because of the instability of the incipient late metal (TPB)Cu–O oxido/oxyl species.[68]

Among the LRu(II,III) species evaluated we found highly exergonic reaction energies (ΔG_{OT} > −40 kcal mol^{-1}) for the two Ru(II) derivatives L = POR/imid (**10a**), salen/imid (**14b**) and a moderate one (ΔG_{OT} −29.5 kcal mol^{-1}) for the Ru(III) derivative **14a** (producing a (POR)ClRu(V)O species). Although the ΔG_a values to form the LRu^{II}-$\overline{O}N_2$ intermediates are somewhat unfavorable (*ca.* +3 kcal mol^{-1}; Table 2), the ΔG^*_{OT} activation barriers of 16.5 and 17.3 kcal mol^{-1} and a ΔG^*_{span} of *ca.* 20 kcal mol^{-1} for N–O cleavage are 10–15 kcal mol^{-1} *lower* than for the corresponding (POR, salen)Fe(II) species. This substantial barrier lowering, predicts far more facile O-transfer reactivity with N_2O for planar LRu(II) species, which is consistent with the room temperature reaction of Ru(POR)(THF) with N_2O to produce (TMP)RuO_2.[36] The corresponding (salen)Ru(III)Cl species **14a** shows a comparable binding energy ΔG_a to the Ru(II) species, but displays a significantly higher activation energy for O-transfer, $\Delta G^*_{OT} = 21\,\text{kcal mol}^{-1}$ and $\Delta G^*_{OT\,span} = 24\,\text{kcal mol}^{-1}$. These barriers for LRu(III) are still about 5 kcal mol^{-1} lower than for the analogous Fe(salen) complexant.

The activation barrier trend among the set of complexants based on the metal ion is as follows, ΔG^*_{OT} : Cr(II) ≤ Ru(II) < Ru(III) < Fe(II). With one apparent exception, the ligand effects on the ease of O–N scission are modest: for the planar ligands: salen ≈ POR ≈ DPDI ≈ salOpr. Anionic complexes of the pyramidal (*N*-3Pyr)M$^-$ (M = Fe, Mn, Cr) generally are calculated to facilitate N–O scission, ΔG^*_{span} ranging from 1–25 kcal mol^{-1}.

Energetics of O-transfer in bimetallics

We now consider the energetics of N_2O binding and N–O O-transfer to the set of selected bimetallic complexes. Note firstly that the exergonic overall O-transfer reaction energy of the mono-metallic counterparts is the same for the pathway through the bimetallic analogs (same net chemical change). With the (salen)Fe species formation of the linear bimetallic complex with N_2O was nearly thermoneutral ΔG_a = +1.1 kcal mol^{-1}, suggesting some possibility for its detection/isolation. This prediction is supported by preliminary experimental observations in our laboratory in which (salen)Fe (**12**)[54f] was found to react with N_2O (5 atm, CH_2Cl_2, rt) as indicated by a burgundy to rust color change and formation of a rust-colored precipitate. Positive ion ESI-MS of the isolated solid showed a prominent ion cluster with a 2Fe isotope pattern centered at *m*/*z* of 689.0782, consistent with a formulation of (salen)Fe-N_2O-Fe(salen) + H^+ (see SI). Formation of the *bent* N_2O-bridged bimetallic complexes with all three planar ligands (*e.g.* **9**, **12**, **15**; Fig. 10) is calculated to be highly endergonic (ΔG_a +20–22 kcal mol^{-1}), so that detection or isolation of such iron complexes is therefore improbable. These high energy bent-bridged intermediates were very close structurally and energe-

tically to the corresponding transition states for N–O scission. Thus, the ΔG^{*}_{OT} for N_2O-bridged **9**, **12** and **15** were remarkably small (1.7–4.1 kcal) with total activation energy spans ΔG^{*}_{span} ($\Delta G_a + \Delta G^{*}_{OT}$) in the moderate range of 22–27 kcal mol^{-1}. The ΔG^{*}_{span} barriers for O–M cleavage *via* the bimetallic complexes are seen to be uniformly lower, −3.5 to −11 kcal mol^{-1}, than those for the corresponding mono-metallic derivatives, LFe(O-N_2), an energy benefit that we term the 'bimetallic advantage', offering a lower energy pathway for N–O cleavage. For the late first row metal species, (TPB)Cu (**5**), the bimetallic energy advantage *via* **5**-N_2O-**5** is especially large, 15.6 kcal mol^{-1} (Table 2), facilitating O–N scission, but this is accompanied by a rather small exergonicity to cleave to the copper-oxyl LCu-O (+LCu(I) + N_2). This probably reflects the instability of late TM oxido/oxyls.[68]

Finally, among the selected Ru(II) and Ru(III) complexes, Ru^{II}(salen)(im)^{s} (**14b**) features exergonic N_2O binding to form the *linear* N_2O-bridged bimetallic **14b**-N_2O-**14b** (ΔG_a −2.6 kcal), a remarkably low activation energy ΔG^{*} of 4.7 kcal mol^{-1} for N–O scission, and a large overall O-transfer exergonicity (−43.6 kcal mol^{-1}). These features, coupled with the very large bimetallic advantage for this system, suggest that the bimetallic N–O cleavage pathway should be especially favorable here relative to the monometallic mechanism. This possibility has been suggested by Groves[36] for the N_2O/Ru(TMP) reaction and by Schomaker[21] in the (TMP)RuO_2-catalyzed N_2O-based alkene epoxidation, but without direct experimental evidence. We note that the entropic price that is paid in forming the bimetallic N_2O-complex is more than counterbalanced by a favorable enthalpic benefit in the N–O cleavage step. This could be a general effect for many metal complexants, as supported by the several examples in Table 2. Finally, we note the *bent* bimetallic LM–N_2O–ML TSs (above) and the bent chromium monometallic (*N*-3Pyr)Cr–O–N_2* species are very similar both structurally in the metal–O–N_2 metrics and energetically – with all having very low activation barriers ΔG^{*}_{OT} of 5–6 kcal mol^{-1}.

Energy profiles for O-transfer pathways

In this last section we display representative reaction energy profiles for the N_2O-transfer reactions of selected complexes in Fig. 15. The reaction pathway in the graphic begins with the N_2O O-coordination by the metal complexant to either the monometallic or bimetallic complex, followed by the O–N cleavage step *via* a transition state (ΔG^{*}) and conversion to the oxido-metal LMO and N_2. Included in Fig. 15 are two planar mono-Fe species, Fe(POR) (**9**) and Fe(salen) (**12**), showing relatively high activation energies for the LFe–O–N_2 cleavage step (27–36 kcal mol^{-1}), with the (POR)Fe species having a somewhat lower barrier. A comparable O–N cleavage barrier (28 kcal mol^{-1}) is seen with the Fe-derivative of the non-planar *N*-2Pyr-Py ligand (**2**). The pyramidal (TPB)Cu (**5**) has a high ΔG^{*}_{O-N} barrier (38 kcal mol^{-1}). On the other hand, the unknown Cr(N-3Pyr)$^{-}$ species (**1d**) shows slightly exergonic N_2O coordination, followed by a remarkably low O–N scission barrier (*ca.*

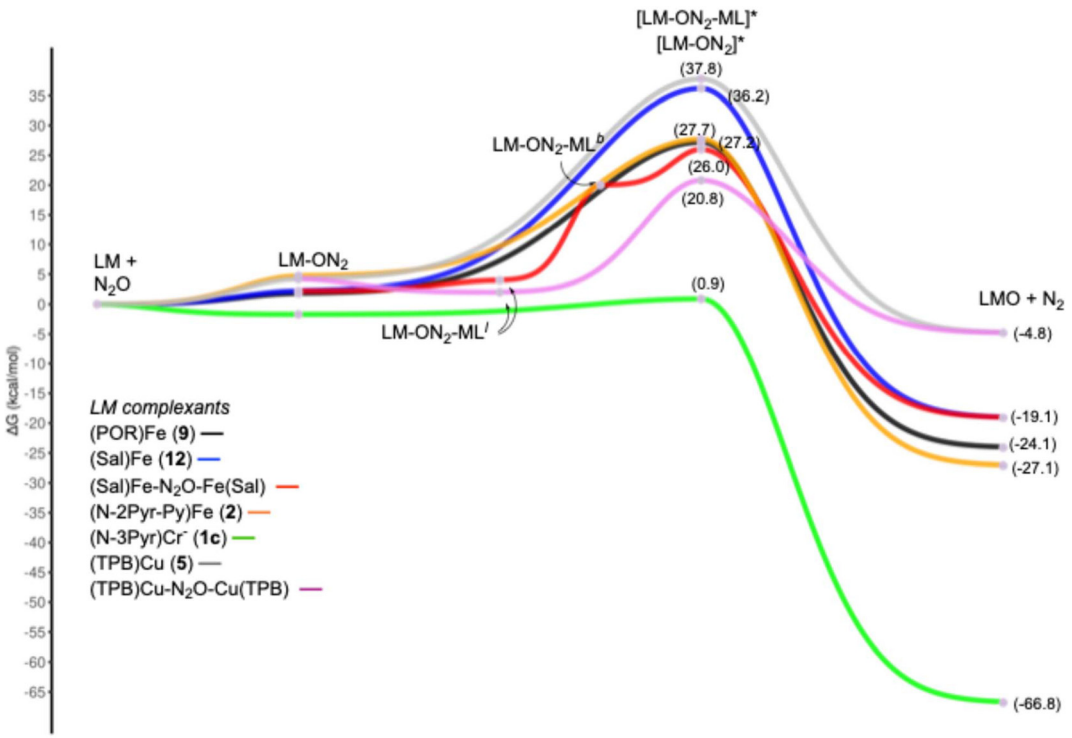

Fig. 15 Energy profiles for the O-transfer reaction pathway of N_2O with selected ligand–metal complexants. Complete energetic data is provided in Table 2.

1 kcal), reflecting the combined effects of an activating ligand and a strongly reducing metal center. The Cr species **1d** also shows the largest overall exergonicity for O-transfer among the monometallic complexants. Also illustrated in Fig. 15 is the substantial decrease in the O–N cleavage barrier that accrues to the LFe(II) (L = salen) and LCu(I) (L = TPB) species *via* bridged bimetallic coordination, $\Delta\Delta G^{*}$ *ca.* 10–15 kcal mol^{-1}. The bimetallic advantage is gained mostly from facilitating the O–N scission step.

Conclusions

DFT calculations have been utilized on several transition metal complexants, LM, M = Fe^{II}, Mn^{II}, Cr^{II}, Ru^{II} and Cu^{I}, with common 4/5-coordinate ligands to assess their N_2O binding affinity and the energetics of N–O cleavage to LMO. The key take home lessons from this study are: (1) the N_2O binding affinities (ΔG_a) range from as high as −5 kcal mol^{-1} to moderate (ΔG_a *ca.* 0 kcal) to low (ΔG_a > +5 kcal mol^{-1}) in the order Ru(II) ≥ Cr(II) > Fe(II), Mn(II) for a variety of 4- and 5-coordinate N,O-donor ligands; (2) N-binding of N_2O is generally more stable than O-binding ($\Delta\Delta G_a$ 1–10 kcal mol^{-1}), with the N,O-selectivity decreasing with increasing spin multiplicity of the complexant; (3) N_2O-binding and cleavage is modestly favored by pyramidal ligands; (4) monometallic O-bound complexes LM–ON_2 generally undergo O–N cleavage with moderate-to-high activation energies, ΔG^{*} 23–40 kcal mol^{-1}; (5) detectable bimetallic linear μ-N_2O complexes are energetically viable; (6) the higher energy bent bimetallics feature very low activation energies ΔG^{*}_{OT} for N–O cleavage, 1–5 kcal mol^{-1}; (7) the total activation span energy ΔG^{*}_{span} for bimetallics, *ca.* 20–30 kcal mol^{-1}, averages 5–8 kcal mol^{-1} lower than for monometallic complexants, providing a lower energy pathway for N–O scission.

Based on this computational study we suggest that monometallic LCr(II) and pyramidal L′Fe(II) and Mn(II) (L′ = *N*-3Pyr, *N*-4Py), and (TPB)Cu are among the best prospects for forming isolable/detectable LM–N_2O complexes for first row TMs since they have near zero ΔG_a. Binding should be enhanced at low temperatures (which minimizes the $T\Delta S$ term on ΔG) and with high pressures (>concentration) of N_2O. Isolation of linear N_2O-bridged bimetallic complexes are also possible for many of these complexants and with the planar LM species. We envision that the deployment of tethered binucleating ligands could further stabilize these by minimizing the entropic cost in the N_2O-association step. The computational evidence for a bimetallic energy advantage for N–O scission supports a role for multi-centered catalysis in metal-zeolite and N_2OR catalytic processes of N_2O. Experimental investigations are underway with a collaborative team at the University of Oklahoma and Toulouse University (FR) to test the efficacy of these high priority systems for reactivity with N_2O and to design next generation complexes that facilitate N–O cleavage through bimetallic activation. Finally, we will report soon on the second phase of the development of nitrous oxide based catalytic oxidations, focusing on identifying the pathways and energetics of hydrocarbon reactions with N_2O-derived oxo-metals.

This contribution provides a number of fundamental, broader insights into the potential development of catalytic reactions of nitrous oxide. Structure–reactivity relationships have been established for several activating metal–ligand complexants (LM) with favorable N_2O binding (the first step in activation/catalysis) and for N–O bond scission leading to oxidizing LM=O species. By evaluating the O–N scission *via* likely experimentally undetectable N_2O–M bonded species, we have identified LCr(II) agents that should adopt novel bent M–O–N_2 structures with very low barriers to N–O scission. We also documented the energetic benefits of *bimetallic complexants* for N_2O binding and N–O cleavage, underscoring the importance of bifunctional activation in FLP-systems, the Cu-enzyme nitrous oxide reductase (N_2OR) and Cu-zeolite diesel N_2O-abatement (heterogeneous) catalysts and (4) we document the influence of the spin states of first-row transition metal complexants on reactivity—an aspect that has only recently been addressed in a few DFT reactivity studies and is relevant to natural and synthetic metallohydroxylases. Moreover, the study advances sustainability and green chemistry by identifying prospective earth-abundant catalysts for N_2O-based oxidations, which, to date, have only been demonstrated with a precious metal (Ru). Finally, the insights into nitrous oxide reactivity—a potent greenhouse gas and underutilized chemical resource—is of significant interest to the catalysis community and may contribute to a deeper understanding of catalytic design strategies.

Data availability

The data supporting this article have been included as part of the supplementary information (SI). Supplementary information is available. See DOI: https://doi.org/10.1039/d6dt01002d.

Conflicts of interest

There are no conflicts of interest to declare.

Acknowledgements

K. N. is grateful for partial support of this project from the National Science Foundation (CHE 1566213 and 2535175), from an A. C. Cope Scholar Award and from the University of Oklahoma (Faculty Development Award and the OU Supercomputing Center for Education and Research). Helpful inputs and discussions with Drs I. Sharma and Y. Shao and Messrs. Chance Lander and Deacon Herndon are also gratefully acknowledged.

References

1 (*a*) S. Saud, D. Wang and S. Fahad, Biology sources of N_2O; Improved nitrogen use efficiency and greenhouse gas emissions in agricultural soils as producers of Biological nitrification inhibitors, *Front. Plant Sci.*, 2022, **13**, 854195; (*b*) T. Arumugham, J. Khudzari, N. Abdullah, A. Yuzir, K. Iwamoto and K. Homma, Research trends and future directions on nitrification and denitrification processes in biological nitrogen removal, *J. Environ. Chem. Eng.*, 2024, **12**, 111897; (*c*) S. Kothari, S. D. Pradeep, M. K. Thammaiah, S. Nithin, T. G. S. Reddy, G. Suresh and D. M. Hithashree, *Pharma Innovation*, 2022, **11**, 447–451; (*d*) Y.-J. Lee, B.-L. Lin and Z. Lei, Nitrous oxide emission mitigation from biological wastewater treatment - A review, *Bioresour. Technol.*, 2022, **362**, 127747.

2 (*a*) L. Chmielarz, Catalytic Methods for Purification of Exhaust Gases Produced by Ammonia-Fueled Engines, *ChemCatChem*, 2025, **17**, e00768; (*b*) Z. Zhuang, B. Guan, J. Chen, C. Zheng, J. Zhou, T. Su, Y. Chen, C. Zhu, X. Hu, S. Zhao, *et al.* Review of nitrous oxide direct catalytic decomposition and selective catalytic reduction catalysts, *Chem. Eng. J.*, 2024, **486**, 150374.

3 (*a*) J. Rios, J. Lebeau, T. Yang, S. Li and M. D. Lynch, A critical review on the progress and challenges to a more sustainable, cost competitive synthesis of adipic acid, *Green Chem.*, 2021, **23**, 3172–3190; (*b*) A. Shimizu, K. Tanaka and M. Fujimori, Abatement technologies for N_2O emissions in the adipic acid industry, *Chemosphere: Global Change Sci.*, 2000, **2**, 425–434.

4 H. Di, A. H. Krichels, M. Trimmer, M. S. M. Jetten and F. E. Loffler, Nitrous oxide sources, mechanisms and mitigation, *Nat. Rev. Earth Environ.*, 2025, **6**, 574–592.

5 NIST Chemistry WebBook, https://webbook.nist.gov/chemistry/bh-ser/.

6 (*a*) K. Rafiq, M. Sabir, I. Sadia, M. Z. Abid, M. A. Nadeem and E. Hussain, Insights into N_2O decomposition in environmental catalysis: evaluation and an advanced outlook, *Mater. Adv.*, 2025, **6**, 8239–8276; (*b*) X. Wu, J. Du, Y. Gao, H. Wang, C. Zhang, R. Zhang, H. He, G. Lu and Z. Wu, Progress and challenges in nitrous oxide decomposition and valorization, *Chem. Soc. Rev.*, 2024, **53**, 8379–8423; (*c*) Y. Zhang, Z. Tian, L. Huang, H. Fan, Q. Hou, P. Cui and W. Wang, Advances in Catalytic Decomposition of N_2O by Noble Metal Catalysts, *Catalysts*, 2023, **13**, 943.

7 (*a*) J. Han, D. Li and J. Yu, Tailoring Cu-based small-pore zeolites towards NH -SCR for NO abatement, *Chem. Soc. Rev.*, 2025, **54**, 7933–7965; (*b*) R. A. Shoonheydt, P. Vanelderen and B. F. Sels, Direct catalytic decomposition of N_2O over Cu- and Fe-zeolites, in *New and Future Developments in Catalysis: Catalysis for Remediation and Environmental Concerns*, ed. S. L. Suib, 2013, pp. 399–419.

8 M.-L. Tsai, R. G. Hadt, P. Vanelderen, B. F. Sels, R. A. Schoonheydt and E. I. Solomon, $[Cu_2O]^{2+}$ Active Site Formation in Cu–ZSM-5: Geometric and Electronic Structure Requirements for N_2O Activation, *J. Am. Chem. Soc.*, 2014, **136**, 3522–3529.

9 M. L. Bols, B. E. R. Snyder, H. M. Rhoda, P. Cnudde, G. Fayad, R. A. Schoonheydt, V. Van Speybroeck, E. I. Solomon and B. F. Sels, Coordination and activation of nitrous oxide by iron zeolites, *Nat. Catal.*, 2021, **4**, 332–340.

10 K. M. Nicholas, C. Lander and Y. Shao, Computational Evaluation of Potential Molecular Catalysts for Nitrous Oxide Decomposition, *Inorg. Chem.*, 2022, **61**, 14591–14605.

11 S. R. Pauleta, S. Dell'Acqua and I. Moura, Nitrous oxide reductase, *Coord. Chem. Rev.*, 2013, **257**, 332–349.

12 A. Pomowski, W. G. Zumft, P. M. Kroneck and O. Einsle, N_2O binding at a [4Cu: 2S] copper–sulphur cluster in nitrous oxide reductase, *Nature*, 2011, **477**, 234–237.

13 Y. Liu, S. Chatterjee, G. E. Cutsail III, S. Peredkov, S. K. Gupta, S. Dechert, S. DeBeer and F. Meyer, Cu_4S Cluster in "0-Hole" and "1-Hole" States: Geometric and Electronic Structure Variations for the Active CuZ* Site of N_2O Reductase, *J. Am. Chem. Soc.*, 2023, **145**, 18477–18486.

14 (*a*) J. Johnson and N. P. Mankad, Model Compounds of Copper-Containing Enzymes Involved in Bacterial Denitrification, *RSC Metallobiology, Series No. 9, Metalloenzymes in Denitrification: Applications and Environmental Impacts*, ed. I. Moura, J. J. G. Moura, S. R. Paulet and L. B. Maia, Royal Society of Chemistry, 2017, ch. 10; (*b*) J. Johnson, W. E. Antholine, S. V. Lindeman, M. J. Graham and N. P. Mankad, A One-Hole Cu4S Cluster with N_2O Reductase Activity: A Structural and Functional Model for Cu Z*, *J. Am. Chem. Soc.*, 2016, **138**, 13107–13110.

15 I. Bar-Nahum, A. K. Gupta, S. M. Huber, M. Z. Ertem, C. J. Cramer and W. B. Tolman, Reduction of nitrous oxide to dinitrogen by a mixed valent tricopper-disulfido cluster, *J. Am. Chem. Soc.*, 2009, **131**, 2812–2814.

16 (*a*) R. Zeng, M. Feller, Y. Ben-David and D. Milstein, Hydrogenation and Hydrosilylation of Nitrous Oxide Homogeneously Catalyzed by a Metal Complex, *J. Am. Chem. Soc.*, 2017, **139**, 5720–5723; (*b*) S. Escayola, M. Sola and A. Poater, Mechanism of the Facile Nitrous Oxide Fixation by Homogeneous Ruthenium Hydride Pincer Catalysts, *Inorg. Chem.*, 2020, **59**, 9374–9383.

17 (*a*) V. Rosca, M. Duca, M. T. de Groot and M. T. M. Koper, Nitrogen Cycle Electrocatalysis, *Chem. Rev.*, 2009, **109**, 2209–2244; (*b*) J. S. Stanley, X. S. Wang and J. Y. Yang, Selective Electrocatalytic Reduction of Nitrous Oxide to Dinitrogen with an Iron Porphyrin Complex, *ACS Catal.*, 2023, **13**, 12617–12622.

18 J. P. Collman, M. Marrocco, C. M. Elliott and M. L'Her, Electrocatalysis of nitrous oxide reduction: Comparison of several porphyrins and binary "face-to-face" porphyrins, *J. Electroanal. Chem. Interfacial Electrochem.*, 1981, **124**, 113–131.

19 K. Hashimoto, H. Tanaka, T. Ikeno and T. Yamada, Selective nitrous oxide oxidation for C-H oxidation and aro-

matization of 9, 10-dihydroanthracene derivatives, *Chem. Lett.*, 2002, **31**, 582–583.

20 K. Hashimoto, Y. Kitaichi, H. Tanaka, T. Ikeno and T. Yamada, Nitrous oxide oxidation of secondary and benzylic alcohols using ruthenium complex catalyst, *Chem. Lett.*, 2001, **30**, 922–923.

21 R. D. Grigg and J. M. Schomaker, Mechanistic Insights into Ru-catalyzed Alkene Epoxidation with Nitrous Oxide as a Terminal Oxidant, *Eur. J. Inorg. Chem.*, 2024, **27**, e202300782.

22 (*a*) A. Mateos-Calbet, P. C. Bruzzese, M. A. Mermigki, A. Schnegg, D. A. Pantazis and J. Cornella, Rapid Oxygen Atom Transfer at a Catalysis-Relevant Ni(I)-Alkyl Complex with N_2O, *J. Am. Chem. Soc.*, 2025, **147**, 19438–19443; (*b*) S. Ni, F. L. Vaillant, A. Mateos-Calbet, R. Martin and J. Cornella, Ni-Catalyzed Oxygen Transfer from N_2O onto sp^3-Hybridized Carbons, *J. Am. Chem. Soc.*, 2022, **144**, 18223–18228; (*c*) F. L. Vaillant, A. Mateos-Calbet, S. Gonzalez-Pelayo, E. J. Reijerse, S. Ni, J. Busch and J. Cornella, Catalytic synthesis of phenols with nitrous oxide, *Nature*, 2022, **604**, 677–683; (*d*) S. Yao and M. Dreiss, Lessons from Isolable Nickel(I) Precursor, Complexes for Small Molecule Activation, *Acc. Chem. Res.*, 2012, **45**, 276–287.

23 K. Severin, Synthetic chemistry with nitrous oxide, *Chem. Soc. Rev.*, 2015, **44**, 6375–6386.

24 (*a*) W. Wislicenus, *Ber. Dtsch. Chem. Ges.*, 1892, **25**, 2084; (*b*) J. Haase, in *Organic Azides, Syntheses and Applications*, ed. S. Brase and K. Banert, Wiley & Sons, Weinheim, 2010, pp. 29–51.

25 S. P. Singh, D. Herndon, U. Chatterjee, K. M. Nicholas and I. Sharma, Investigating the reactivity of nitrous oxide with lithiated hydrazines: application to the synthesis of diarylethanes from diarylmethylhydrazines, *New J. Chem.*, 2025, **49**, 1182–1188.

26 F. M. Beringer, J. A. Farr Jr. and S. Sands, The Reactions of Nitrous Oxide with Organolithium Compounds, *J. Am. Chem. Soc.*, 1953, **75**, 3984–3987.

27 (*a*) A. G. Tskhovrebov, E. Solari, M. Wodrich, R. Scopelliti and K. Severin, Covalent capture of nitrous oxide by N-heterocyclic carbenes, *Angew. Chem., Int. Ed.*, 2012, **51**, 232; (*b*) A. G. Tskhovrebov, B. Vuichoud, E. Solari, R. Scopelliti and K. Severin, Adducts of nitrous oxide and N-heterocyclic carbenes: syntheses, structures, and reactivity, *J. Am. Chem. Soc.*, 2013, **135**, 9486; (*c*) M. Gohner, P. Haiss, N. Kuhn, M. Strobele and K.-P. Zeller, The 1: 1 Adduct of 1,3-Diisopropyl-4,5-dimethyl-2,3-dihydroimidazol-2-ylidene and Nitrous Oxide, *Z. Naturforsch.*, 2013, **68b**, 539; (*d*) E. Theuergarten, T. Bannenberg, M. D. Walter, D. Holschumacher, M. Freytag, C. G. Daniliuc, P. G. Jones and M. Tamm, Computational and experimental investigations of CO_2 and N_2O fixation by sterically demanding N-heterocyclic carbenes (NHC) and NHC/borane FLP systems, *Dalton Trans.*, 2014, **43**, 1651.

28 S. Poh, R. Hernandez, M. Inagaki and P. G. Jessop, Oxidation of Phosphines by Supercritical Nitrous Oxide, *Org. Lett.*, 1999, **1**, 583.

29 (*a*) Z. Mo, E. L. Kolychev, A. Rit, J. Campos, H. Niu and S. Aldridge, Facile Reversibility by Design: Tuning Small Molecule Capture and Activation by Single Component Frustrated Lewis Pairs, *J. Am. Chem. Soc.*, 2015, **137**, 12227–12230; (*b*) D. W. Stephan and G. Erker, Frustrated Lewis pair chemistry of carbon, nitrogen and sulfur oxides, *Chem. Sci.*, 2014, **5**, 2625–2641; (*c*) E. Otten, R. C. Neu and D. W. Stephan, Complexation of nitrous oxide by frustrated Lewis pairs, *J. Am. Chem. Soc.*, 2009, **131**, 9918–9919; (*d*) R. C. Neu, E. Otten and D. W. Stephan, Bridging Binding Modes of Phosphine-Stabilized Nitrous Oxide to $Zn(C_6F_5)_2$, *Angew. Chem., Int. Ed.*, 2009, **48**, 9709; (*e*) G. Mecalard, J. A. Hatnean, H. J. Cowley, A. J. Lough, J. M. Rawson and D. W. Stephan, C–H Bond Activation by Radical Ion Pairs Derived from $R_3P/Al(C_6F_5)_3$ Frustrated Lewis Pairs and N_2O, *J. Am. Chem. Soc.*, 2013, **135**, 6446.

30 (*a*) W. B. Tolman, Binding and Activation of N_2O at Transition-Metal Centers: Recent Mechanistic Insights, *Angew. Chem., Int. Ed.*, 2010, **49**, 1018–1024; (*b*) K. Severin, Homogeneous catalysis with nitrous oxide, *Trends Chem.*, 2023, **5**, 574–576.

31 (*a*) J. Armor and H. Taube, Reduction of nitrous oxide in the presence of pentaammine-aquoruthenium(II), *J. Am. Chem. Soc.*, 1971, **93**, 6476–6480; (*b*) V. Zhuravlev and P. J. Malinowski, A Stable Crystalline Copper(I)–N_2O Complex Stabilized as the Salt of a Weakly Coordinating Anion, *Angew. Chem.*, 2018, **130**, 11871–11874; (*c*) N. A. Piro, M. F. Lichterman, W. H. Harman and C. J. Chang, A structurally characterized nitrous oxide complex of vanadium, *J. Am. Chem. Soc.*, 2011, **133**, 2108–2111; (*d*) M. R. Gyton, B. Leforestier and A. B. Chaplin, Rhodium(I) Pincer Complexes of Nitrous Oxide, *Angew. Chem., Int. Ed.*, 2019, **58**, 15295–15298.

32 (*a*) C. C. Mokhtarzadeh, C. Chan, C. E. Moore, A. L. Rheingold and J. S. Figueroa, Side-On Coordination of Nitrous Oxide to a Mononuclear Cobalt Center, *J. Am. Chem. Soc.*, 2019, **141**, 15003–15007; (*b*) B. M. P. Lombardi, C. Gendy, B. S. Gelfand, G. M. Bernard, R. E. Wasylishen, H. M. Tuononen and R. Roesler, Side-on Coordination in Isostructural Nitrous Oxide and Carbon Dioxide Complexes of Nickel, *Angew. Chem., Int. Ed.*, 2021, **60**, 7077–7081.

33 (*a*) F. Bottomley, I. J. B. Lin and M. Mukaida, Reactions of dinitrogen oxide (nitrous oxide) with dicyclopentadienyltitanium complexes including a reaction in which carbon monoxide is oxidized, *J. Am. Chem. Soc.*, 1980, **102**, 5238; (*b*) F. Bottomley and H. Brinzinger, Reactions of nitrogen oxides with di(cyclopentadienyl)titanium complexes, *J. Chem. Soc., Chem. Commun.*, 1978, 234.

34 T. D. Palluccio, E. V. Rybak-Akimova, S. Majumdar, M. Cai, X. Chui, M. Temprado, J. S. Silvia, A. F. Cozzolino, D. Tofan, A. Velian, C. C. Cummins, B. Captain and C. D. Hoff, Thermodynamic and Kinetic Study of Cleavage of the N–O Bond of *N*-Oxides by a Vanadium(III) Complex: Enhanced Oxygen Atom Transfer Reaction Rates for Adducts of Nitrous Oxide and Mesityl Nitrile Oxide, *J. Am. Chem. Soc.*, 2013, **135**, 11357–11372.

35 (*a*) S. M. Franke, B. L. Tran, F. W. Heinemann, W. Hieringer, D. J. Mindiola and K. Meyer, Uranium(III) complexes with bulky aryloxide ligands featuring metal–arene interactions and their reactivity toward nitrous oxide, *Inorg. Chem.*, 2013, **52**, 10552; (*b*) L. R. Avens, D. M. Barnhart, C. J. Burns, S. D. McKee and W. H. Smith, Oxidation chemistry of a uranium(III) aryloxide, *Inorg. Chem.*, 1994, **33**, 4245.

36 J. T. Groves and J. S. Roman, Nitrous oxide activation by a ruthenium porphyrin, *J. Am. Chem. Soc.*, 1995, **117**, 5594–5595.

37 (*a*) K. Koo and G. L. Hillhouse, Formation of a substituted tetrahydrofuran by formal [2 + 2 + 1] coupling of an oxygen atom with two olefins at a nickel center, *Organometallics*, 1998, **17**, 2924–2925; (*b*) K. Koo, G. L. Hillhouse and A. L. Rheingold, Oxygen-atom transfer from nitrous oxide to an organonickel(II) phosphine complex. Syntheses and reactions of new nickel(II) aryloxides and the crystal structure of [cyclic] (Me2PCH2CH2PMe2)Ni(O-o-C6H4CMe2CH2), *Organometallics*, 1995, **14**, 456–460; (*c*) D. J. Mindiola, L. A. Watson, K. Meyer and G. L. Hillhouse, Functionalization of Complexed N_2O in Bis(pentamethylcyclopentadienyl) Systems of Zirconium and Titanium, *Organometallics*, 2014, **33**, 2760–2769; (*d*) N. D. Harrold, R. Waterman, G. L. Hillhouse and T. R. Cundari, Group-Transfer Reactions of Nickel-Carbene and -Nitrene Complexes with Organoazides and Nitrous Oxide that Form New C : N, C : O and N : N Bonds, *J. Am. Chem. Soc.*, 2009, **131**, 12872–12873; (*e*) P. T. Matsunaga, J. C. Mavropoulos and G. L. Hillhouse, Oxygen-atom transfer from nitrous oxide to nickel alkyls. Syntheses and reactions of nickel(II) alkoxides, *Polyhedron*, 1995, **14**, 175–185.

38 (*a*) F. Furche and J. P. Perdew, The Performance of Semilocal and Hybrid Density Functionals in 3d Transition-Metal Chemistry, *J. Chem. Phys.*, 2006, **124**, 044103; (*b*) O. Salomon, M. Reiher and B. A. Hess, Assertion and validation of the performance of the B3LYP* functional for the first transition metal row and the G2 test set, *J. Chem. Phys.*, 2002, **117**, 4729–4737; (*c*) T. Weymuth, E. P. A. Couzijn, P. Chen and M. Reiher, New Benchmark Set of Transition-Metal Coordination Reactions for the Assessment of Density Functionals, *J. Chem. Theory Comput.*, 2014, **10**, 3092–3103.

39 (*a*) M. Radon, G. Drabik, M. Hodorowicz and J. Szklarzewicz, Performance of quantum chemistry methods for a benchmark set of spin-state energetics derived from experimental data of 17 transition metal complexes (SSE17), *Chem. Sci.*, 2024, **15**, 20189–20204; (*b*) E. Gera and K. R. Vignesh, A systematic comparison of density functional methods for determining spin-state energy gaps and spin transition temperature of spin crossover complexes, *RSC Adv.*, 2026, **16**, 2241–2254.

40 (*a*) P. Verma, Z. Varga, J. E. M. N. Klein, C. J. Cramer, L. Que Jr. and D. G. Truhlar, Assessment of electronic structure methods for the determination of the ground spin states of Fe(II), Fe(III) and Fe(IV) complexes, *Phys. Chem. Chem. Phys.*, 2017, **19**, 13049–13069; (*b*) H. Hirao, D. Kumar, L. Que Jr. and S. Shaik, Two-State Reactivity in Alkane Hydroxylation by Non-Heme, Iron-Oxo Complexes, *J. Am. Chem. Soc.*, 2006, **128**, 8590–8860; (*c*) L. d. S. da Silva, F. C. S. Soares, A. A. de Souza and É. Sá, DFT Benchmarking for Fe(II)-(Alkyl/Alkylidene/Acetylide) Complexes, *ACS Omega*, 2025, **10**, 61169–61178.

41 (*a*) M. Swart and M. Gruden, Spinning around in Transition-Metal Chemistry, *Acc. Chem. Res.*, 2016, **49**, 2690–2697; (*b*) F. Shahbazi-Raz, M. Adineh, N. Safari and M. Zahedi, Theoretical calculation and prediction for experimental design to obtain spin crossover complexes, *Int. J. Quantum Chem.*, 2016, **116**, 1179–1186; (*c*) M. Swart, A. W. Ehlers and K. Lammertsma, Performance of the OPBE exchange-correlation functional, *Mol. Phys.*, 2004, **102**, 2467–2474.

42 (*a*) E. Gera and K. R. Vignesh, A systematic comparison of density functional methods for determining spin-state energy gaps and spin transition temperature of spin crossover complexes, *RSC Adv.*, 2026, **16**, 2241–2254; (*b*) P. He and S.-F. Zhu, Spin Crossover and Its Application in Organometallic Catalysis: Concepts and Recent Progress, *Chem. – Eur. J.*, 2024, **30**, e202403437; (*c*) M. Radon, Benchmarks for transition metal spin-state energetics: why and how to employ experimental reference data, *Phys. Chem. Chem. Phys.*, 2023, **25**, 30800–30820; (*d*) I. D. Dergachev, V. D. Dergachev, M. Rooein, A. Mirzanejad and S. A. Varganov, Predicting Kinetics and Dynamics of Spin-Dependent Processes, *Acc. Chem. Res.*, 2023, **56**, 856–866.

43 M. J. Frisch, G. W. Trucks, H. B. Schlegel, G. E. Scuseria, M. A. Robb, J. R. Cheeseman, G. Scalmani, V. Barone, G. A. Petersson, H. Nakatsuji, X. Li, M. Caricato, A. V. Marenich, J. Bloino, B. G. Janesko, R. Gomperts, B. Mennucci, H. P. Hratchian, J. V. Ortiz, A. F. Izmaylov, J. L. Sonnenberg, D. Williams-Young, F. Ding, F. Lipparini, F. Egidi, J. Goings, B. Peng, A. Petrone, T. Henderson, D. Ranasinghe, V. G. Zakrzewski, J. Gao, N. Rega, G. Zheng, W. Liang, M. Hada, M. Ehara, K. Toyota, R. Fukuda, J. Hasegawa, M. Ishida, T. Nakajima, Y. Honda, O. Kitao, H. Nakai, T. Vreven, K. Throssell, J. A. Montgomery Jr., J. E. Peralta, F. Ogliaro, M. J. Bearpark, J. J. Heyd, E. N. Brothers, K. N. Kudin, V. N. Staroverov, T. A. Keith, R. Kobayashi, J. Normand, K. Raghavachari, A. P. Rendell, J. C. Burant, S. S. Iyengar, J. Tomasi, M. Cossi, J. M. Millam, M. Klene, C. Adamo, R. Cammi, J. W. Ochterski, R. L. Martin, K. Morokuma, O. Farkas, J. B. Foresman and D. J. Fox, *Gaussian 16*, Gaussian Inc., Wallingford, CT, 2016.

44 (*a*) A. D. Becke, A new mixing of Hartree-Fock and local density-functional theories, *J. Chem. Phys.*, 1993, **98**, 1372–1377; (*b*) J. P. Perdew, M. Ernzerhof and K. Burke, Rationale for mixing exact exchange with density functional approximations, *J. Chem. Phys.*, 1996, **105**, 9982–

9985; (*c*) K. Kim and K. D. Jordan, Comparison of Density Functional and MP2 Calculations on the Water Monomer and Dimer, *J. Phys. Chem.*, 1994, **98**, 10089–10094.

45 P. J. Hay and W. R. Wadt, Ab Initio Effective Core Potentials for Molecular Calculations. Potentials for K to Au Including the Outermost Core Orbitals, *J. Chem. Phys.*, 1985, **82**, 299–310.

46 (*a*) R. Ditchfield, W. J. Hehre and J. A. Pople, Self-Consistent Molecular-Orbital Methods. IX. An Extended Gaussian-Type Basis for Molecular-Orbital Studies of Organic Molecules, *J. Chem. Phys.*, 1971, **54**, 724–728; (*b*) W. J. Hehre, R. Ditchfield and J. A. Pople, Self-Consistent Molecular Orbital Methods. XII. Further Extensions of Gaussian-Type Basis Sets for Use in Molecular Orbital Studies of Organic Molecules, *J. Chem. Phys.*, 1972, **56**, 2257–2261; (*c*) P. C. Hariharan and J. A. Pople, The Influence of Polarization Functions on Molecular Orbital Hydrogenation Energies, *Theor. Chim. Acta*, 1973, **28**, 213–222.

47 (*a*) S. Grimme, J. Antony, S. Ehrlich and H. J. Krieg, *Chem. Phys.*, 2010, **132**, 154104; (*b*) T. Husch, L. Freitag and M. Reiher, Calculation of Ligand Dissociation Energies in Large Transition-Metal Complexes, *J. Chem. Theory Comput.*, 2018, **14**, 2456–2468; (*c*) M. Bursch, E. Caldeweyher, A. Hansen, H. Neugebauer, S. Ehlert and S. Grimme, Understanding and Quantifying London Dispersion Effects in Organometallic Complexes, *Acc. Chem. Res.*, 2019, **52**, 258–266.

48 A. V. Marenich, C. J. Cramer and D. G. Truhlar, Universal Solvation Model Based on Solute Electron Density and on a Continuum Model of the Solvent Defined by the Bulk Dielectric Constant and Atomic Surface Tensions, *J. Phys. Chem. B*, 2009, **113**, 6378–6396.

49 Y. Zhao and D. G. Truhlar, The M06 suite of density functionals for main group thermochemistry, thermochemical kinetics, noncovalent interactions, excited states, and transition elements: two new functionals and systematic testing of four M06-class functionals and 12 other functionals, *Theor. Chem. Acc.*, 2008, **120**, 215–241.

50 X. Li and M. J. Frisch, Energy-Represented Direct Inversion in the Iterative Subspace within a Hybrid Geometry Optimization Method, *J. Chem. Theory Comput.*, 2006, **2**, 835–839.

51 G. Knizia, Intrinsic Atomic Orbitals: An Unbiased Bridge between Quantum Theory and Chemical Concepts, *J. Chem. Theory Comput.*, 2013, **9**, 4834–4843.

52 M. K. Bogdos and B. Morandi, *EveRplot*: A Web-Based Shiny Application for Creating Energy vs Reaction Coordinate Diagrams, *Chem. Educ.*, 2023, **100**, 3641–3644.

53 (*a*) R. H. Holm, Metal-Centered Oxygen Atom Transfer Reactions, *Chem. Rev.*, 1987, **87**, 1401–1449; (*b*) L. Que Jr., The Road to Non-Heme Oxoferryls and Beyond, *Acc. Chem. Res.*, 2007, **40**, 493–500; (*c*) W. Nam, Y.-M. Lee and S. Fukuzumi, Hydrogen Atom Transfer Reactions of Mononuclear Nonheme Metal-Oxygen Intermediates, *Acc. Chem. Res.*, 2018, **51**, 2014–2022; (*d*) W. Li, R. Tang, S. Xiong, L. Li, Z. Zhou, L. Su, D. Gong and Y. Deng, High-valent metal-oxo species in catalytic oxidations for environmental remediation and energy conversion, *Coord. Chem. Rev.*, 2024, **510**, 215840; (*e*) S. Fukuzumi, Electron transfer and catalysis with high-valent metal-oxo complexes, *Dalton Trans.*, 2015, **44**, 6696; (*f*) C.-M. Che, V. K.-Y. Lo, C.-Y. Zhou and J.-S. Huang, Selective functionalisation of saturated C–H bonds with metalloporphyrin catalysts, *Chem. Soc. Rev.*, 2011, **40**, 1950–1975; (*g*) O. Y. Lyakina and A. A. Shteinman, Oxo Complexes of High-Valence Iron in Oxidation Catalysis, *Kinet. Catal.*, 2012, **53**, 694–713; (*h*) J. T. Groves, in *Cytochrome P450: Structure, Mechanism, and Biochemistry*, ed. P. R. Ortiz de Montellano, Kluwer-Academic/Plenum, New York, 3rd edn, 2005, pp. 1.

54 (*a*) R. N. Mukherjee, A. J. Abrahamson, G. S. Patterson, T. D. P. Stack and R. H. Holm, A New Class of Five-Coordinate [Fe(salen)L] Complexes: Preparation, Properties, and Mechanism of Electron-Transfer Reactions, *Inorg. Chem.*, 1988, **27**, 2137–2144; (*b*) H. M. Hüppe, L. Iffland-Mühlhaus, J. Heck, M. Eilers, H. Gildenast, S. Schönfeld, A. Dürrmann, A. Hoffmann, B. Weber, U.-P. Apfel and S. Herres-Pawli, Triflate vs Acetonitrile: Understanding the Iron(II)-Based Coordination Chemistry of Tri(quinolin-8-yl)amine, *Inorg. Chem.*, 2023, **62**, 4435–4455; (*c*) P. L. Holland, All square for high-spin iron(II), *Nat. Chem.*, 2011, **3**, 507–508; (*d*) J. P. Collman, J. L. Hoard, N. Kim, G. Lang and C. A. Reed, *J. Am. Chem. Soc.*, 1975, **97**, 2676–2681; (*e*) J. Lewis, F. E. Mabbs and H. Weigold, The Magnetic Properties of Some Manganese(II) Schiff-base Complexes and the Oxidation Products of N,N'-Ethylenebis (salicylaldiminato)manganese(II), *J. Chem. Soc. A*, 1968, 1699–1703; (*f*) A. Earnshaw, E. A. King and L. F. Larkworthy, Transition Metal-Schiff's Base Complexes. Part 1V. Iron(II) and Manganese(II) Systems, *J. Chem. Soc. A*, 1968, 1048–1049; (*g*) S. K. Cheung, C. J. Grimes, J. Wong and C. A. Reed, Chromium(II) Porphyrins and an Irreversible Dioxygen Complex, *J. Am. Chem. Soc.*, 1976, **98**, 5028–5030.

55 C. P. Rinsland, M. A. H. Smith, A. Goldman, V. M. Devi and D. C. Benner, Parameters for the measurement of the spectral features of the $\nu1$, $\nu2$, $\nu3$ bands of $^{14}N_2{}^{16}O$, *J. Quant. Spectrosc. Radiat. Transfer*, 1992, **48**, 533–542.

56 M. Knapp, O. Echt, D. Kreisle, T. D. Mark and E. Recknag, Formation of long-lived CO2-, N_2O- and their dimer anions by electron attachment to van der Waals clusters, *Chem. Phys. Lett.*, 1986, **126**, 225–231.

57 J. N. Armor and H. Taube, Evidence of a Binuclear Nitrous Oxide Complex of Ruthenium, *Chem. Commun.*, 1971, 287.

58 (*a*) S. K. Mahapatra, B. Ghosh and L. Roy, Harnessing Selectivity and Reactivity with Noncovalent Interactions in Molecular and Supramolecular Organo-Catalysis: A Computational Perspective, *ChemCatChem*, 2025, **17**, e01069; (*b*) M. Gray and J. M. Herbert, Density functional theory for van der Waals complexes: size matters, *Annu. Rep. Comput. Chem.*, 2024, **20**, 1–61.

59 K. Fields, B. M. Barngrover and J. B. Gary, Computational Investigation of the Preferred Binding Modes of N_2O in Group 8 Metal Complexes, *Inorg. Chem.*, 2020, **59**, 18314–18318.

60 W. H. Harman and C. J. Chang, N_2O Activation and Oxidation Reactivity from a Non-Heme Iron Pyrrole Platform, *J. Am. Chem. Soc.*, 2007, **129**, 15128–15129.

61 (*a*) A. Caballero, M. M. Diaz-Requejo, M. R. Fructos, J. Urbano, P. J. Ed. Perez, M. Stradiotto and R. J. Lundgren, Modern Applications of Trispyrazolylborate Ligands in Coinage Metal Catalysis, *Ligand Design in Metal Chemistry*, 2016, pp. 308–329; (*b*) C. Martin, J. M. Munoz-Molina, A. Locati, E. Alvarez, F. Maseras, T. R. Belderrain and P. J. Perez, Copper(I)-Olefin Complexes: The Effect of the Trispyrazolylborate Ancillary Ligand in Structure and Reactivity, *Organometallics*, 2010, **29**, 3481–3489; (*c*) T. F. van Dijkman, M. A. Siegler and E. Bouwman, Copper(I) Complexes of Naphthyl-Substituted Fluorinated (Tris)pyrazolylborate Ligands with Ethene and Carbon Monoxide, *Eur. J. Inorg. Chem.*, 2016, 2586–2594.

62 A. Milani and C. Castiglioni, Atomic charges from atomic polar tensors: A comparison of methods, *J. Mol. Struct.: THEOCHEM*, 2010, **955**, 158–164.

63 S. Kozuch and S. Shaik, How to Conceptualize Catalytic Cycles? The Energetic Span Model, *Acc. Chem. Res.*, 2011, **44**, 101–110.

64 A practical reaction temperature can be estimated from the activation free energy ΔG^* and approximate rate constant using the Eyring equation, $T = \Delta G^*/R[\ln(k_{BBT}/hk)]$; R. Chang, *Physical Chemistry for the Biosciences*, University Science Books, USA, 2005, pp. 338–342.

65 (*a*) P. He and S.-F. Zhu, Spin Crossover and Its Application in Organometallic Catalysis: Concepts and Recent Progress, *Chem. – Eur. J.*, 2024, **30**, e202403437; (*b*) M. Radon, Benchmarks for transition metal spin-state energetics: why and how to employ experimental reference data, *Phys. Chem. Chem. Phys.*, 2023, **25**, 30800–30820; (*c*) I. D. Dergachev, V. D. Dergachev, M. Rooein, A. Mirzanejad and S. A. Varganov, Predicting Kinetics and Dynamics of Spin-Dependent Processes, *Acc. Chem. Res.*, 2023, **56**, 856–866.

66 (*a*) T. Skipworth, M. Khashimov, I. Ojo and R. Zhang, Kinetics of chromium(V)-oxo and chromium(IV)-oxo porphyrins: Reactivity and mechanism for sulfoxidation reactions, *J. Inorg. Biochem.*, 2022, **237**, 112006; (*b*) J. T. Groves, W. J. Kruper Jr., R. C. Haushalter and W. M. Butler, Synthesis, characterization, and molecular structure of oxo (porphyrinato)chromium(IV) complexes, *Inorg. Chem.*, 1982, **21**, 1363–1368; (*c*) K. Qin, C. D. Incarvito, A. L. Rheingold and K. H. Theopold, Hydrogen Atom Abstraction by a Chromium(IV) Oxo Complex Derived from O2, *J. Am. Chem. Soc.*, 2002, **124**, 14008–14009.

67 J. S. Roman, *Nitrous Oxide Activation and Thiirane Desulfurization by Metalloporphyrins*, Ph.D. dissertation, Princeton University, Princeton, N.J., 1995.

68 (*a*) Monika, M. Kumar, Somi, A. Sarkar, M. K. Gupta and A. Ansari, Theoretical study of the formation of metal–oxo species of the first transition series with the ligand 14-TMC: driving factors of the "Oxo Wall", *Dalton Trans.*, 2023, **52**, 1416; (*b*) S. Kim, J. Stahlberg, M. Sandgren, R. S. Paton and G. T. Beckham, Quantum mechanical calculations suggest that lytic polysaccharide monooxygenases use a copper-oxyl, oxygen-rebound mechanism, *Proc. Natl. Acad. Sci. U. S. A.*, 2014, **111**, 149–154; (*c*) N. Cao, A. C. Castro, D. Balcells, U. Olsbye and A. Nova, Copper(II)-Oxyl Formation in a Biomimetic Complex Activated by Hydrogen Peroxide: The Key Role of *Trans*-Bis(Hydroxo) Species, *Inorg. Chem.*, 2024, **63**, 23082–23094.